Computers and Structures 242 (2021) 106372

Contents lists available at ScienceDirect

Computers and Structures

journal homepage: www.elsevier.com/locate/compstruc

Numerical limit analysis-based modelling of masonry structures subjected to large displacements

A. Iannuzzo *, A. Dell'Endice, T. Van Mele, P. Block

ETH Zurich, Institute of Technology in Architecture, Block Research Group, Stefano-Franscini-Platz 1, HIB E45, CH-8093 Zurich, Switzerland

ARTICLE INFO

Article history:
Received 12 March 2020
Accepted 23 August 2020

Keywords:
Masonry structures
Unilateral contact
Settlements
Cracks and internal stress states
Limit analysis
Displacement capacity

ABSTRACT

In this paper, we introduce an extension of the piecewise rigid displacement (PRD) method for addressing the stability of a generic two-dimensional masonry structure subjected to large displacements. So far, the PRD method has been applied to simulate cracks in the reference configuration considering small displacements. Here, we investigate both cracks and internal forces in the presence of large foundation displacements, also providing an approach to estimate their maximum allowable value. The proposed extension allows accounting for the evolution of both mechanism and corresponding internal stress state due to the increasing prescribed displacements.

After benchmarking the PRD analysis of a pointed arch with a physical test and results obtained through the Discrete Element Modelling software 3DEC, its strength/use is demonstrated on a complex numerical application, based on the cross-section of a Gothic cathedral. Also in this case, the PRD results are compared with a 3DEC analysis showing good agreement in terms of cracks evolution, internal stress states and displacement capacity. This paper shows the ability of the PRD method in solving in a few seconds a critical issue in the field of masonry structures that is, the effects of large foundation displacements, both in terms of mechanisms and forces, simultaneously.

1. Introduction

Masonry constructions represent a significant portion of the global built inventory and, particularly in Europe, an essential share of the monumental architectural heritage. Understanding the stability of masonry structures under given settlements is a critical issue in the current research field [1], especially because cracks not always represent a risk but rather the natural way used by masonry structures to stably accommodate the external changes of the environment [1–3]. In this sense, fractures are the real manifestation of the ductility of masonry constructions, making them resilient to settlements [4].

Recent years have seen a continuous development of methods and computational tools to assess the stability of masonry structures, in particular under given settlements. Despite this continuous growth of demand for masonry safety assessments, as Como noted in [1], "there is a lack of a widely accepted approach to studying the statics of masonry structures".

Finite elements (FE) approaches have been proposed, applied and benchmarked for the assessment of masonry structures affected by large settlements: [5] applied the FE method to masonry arch bridges, also concluding that the stability is not dominated by material crushing; in [6], full 3D FE analyses were performed to also simulate the foundation-settlement effects of a pile, showing that masonry arch bridges are very ductile, meaning that the structure is supposed to undergo very large settlements before its collapse; in [7], the author proposes an interphase model to simulate the damage propagation in masonry walls within a mesoscopic approach. Beyond the use of FE or scale models [8], other different computational approaches have also been used to predict the effect of foundation displacements, such as discrete element modelling (DEM) [9–13], numerical codes based on rigid spring models [14,15] or rigid block models [16] arising from Livesley's formulation [17] and arranged as in [18] or for large displacement as done in [19]. In [19], modelling the masonry as an assembly of rigid blocks interacting with no-tension, frictional contact interface, the authors propose an incremental force-based approach standing on two linear programming (LP) problems, which can also be linked with the two standard forms of upper and lower bound formulations of limit analysis assuming an associative flow-rule. In particular, the primal variables are forces, solving the static LP problem, while the displacements of the contact points are derived as Lagrange multipliers associated with the first solution.

* Corresponding author.
E-mail addresses: iannuzzo@arch.ethz.ch (A. Iannuzzo), dellendice@arch.ethz.ch (A. Dell'Endice), van.mele@arch.ethz.ch (T. Van Mele), block@arch.ethz.ch (P. Block).

https://doi.org/10.1016/j.compstruc.2020.106372
0045-7949/

As proved by Heyman since 1966 [2], the stability of masonry structures depends directly on their geometry rather than on their strength. Indeed, Heyman gave the theoretical basis for the application of limit analysis (LA) to masonry structures through three clear, but crude, assumptions: (i) masonry has no tensile strength, (ii) masonry has infinite compressive strength, (iii) sliding failure does not occur. Thanks to his contribution, the work done in the past centuries by many scholars found a robust mathematical framework, e.g. [20,21]. While the first two assumptions are derived from masonry mechanical behaviour, the third one, which can also be considered as the most crucial, comes from noting that masonry structures are not a chaotic collection of bricks, but rather a smart and appropriate assemblage that by its nature prevents sliding failures [22–24]. In his work, Heyman studied the arch in detail [25] and extended his analyses to a wide range of masonry structures, particularly Gothic cathedrals [26] and their peculiar structural elements. Nowadays, his theory is accepted as one of the most appropriate ways to assess the stability of masonry structures [1,27–30], capable of catching fractures and zero-energy modes, which other methods, such as the finite element (FE) method, cannot [31,32]. The reliability of the Heyman model in catching stable mechanisms is also proved in [33], where the analysis of the stable mechanisms exhibited by circular arches subjected to generic settlements of one support is proposed.

Large displacement analyses, based on an equilibrium approach, can be found in [34,35], where the author identified the domain of statically admissible movements and defined kinematic safety factors for voussoir arches, or in [4,32,36] for continuous circular arches. Nevertheless, these strategies can be applied only to simple structures or are restricted to cases when the mechanism is qualitatively known in advance. Except for [4,35], many works neglect that the crack pattern, and thus the location of the hinges, can change to accommodate the increased displacement, which is one of the key features of masonry structures undergoing large displacements. This phenomenon has rarely been studied. The first scholars who addressed this study were Ochsendorf in [4] and Smars [35], a recent application can be found in [37] or with a new formulation of the equilibrium approach in [38], but all of them are restricted to arch geometries.

Even though the equilibrium approach has been extensively studied to assess the stability through the Safe Theorem, past efforts to computationally frame the Heyman model for solving the kinematic problem under given displacements have been almost entirely restricted to simple structures for which the qualitative crack pattern is known in advance.

A way to overcome this problem has been shown in [39,40], where an energy criterion has been proposed and applied to solve the kinematical problem for masonry structures composed of normal, rigid no-tension (NRNT) material [41–43]. The constitutive relations defining the NRNT material are equivalent to the ones defining the normality rules [44] and provide a natural way to frame Heyman's model into continuum mechanics [42]. It also captures the peculiar aspect of a masonry structure subjected to settlements, that is, the nucleation of the structure into a finite number of rigid blocks (macroblocks) with cracks appearing as jumps of the displacement fields along their boundaries. Assuming the NRNT models, two variational formulations can be used to solve the kinematic and equilibrium problem for masonry structures: the first one is based on the minimum of the total potential energy (the reader is referred to [40,39] for the proof and to [39] for applications and benchmarks) while the second one is based on the minimum of the complementary energy (see [3] for the proof and an application). The first minimum energy criterion leads to displacement-based methods which can be used to select the rigid macroblock partition. The second one allows defining internal stress states in equilibrium with external loads and compatible with given external displacements. A recent contribution [45] derives the two above mentioned variational formulations as a special case of the Signorini contact problem between multiple no-tension rigid bodies satisfying the NRNT materials assumptions. In [39] two numerical strategies, namely the piecewise rigid displacement (PRD) and C0 method, were proposed to find a solution of the boundary value problem (BVP) for NRNT materials, both leading to linear programming (LP) formulations. The main idea behind both numerical approaches is to catch the rigid macroblock partition exhibited by a masonry structure when subjected to even severe external actions, such as the settlements or seismic actions [46]. The PRD approach constitutes a numerical way to discretise and solve the BVP for NRNT materials in the space of piecewise-rigid, small-displacement fields which intuitively are strictly connected to a rigid macroblock partition of the structural domain.

Conversely, as proposed in [39,47,48], the same energy criterion can be used to solve the BVP in the space of continuous displacement fields but assuming a different numerical strategy, and in this case, the fracture pattern appears as smeared (C0 method). Nonetheless, even though smeared, as shown in [39,47] it allows to catch and select the rigid macroblock partition of the structural domain and also to overcome some mesh-dependencies (see [48] where the two approaches are applied and compared in a real case study).

The PRD approach represents a method to computationally apply Limit Analysis framing the search for a solution as a linear programming (LP) problem where the objective function is the total potential energy of the external loads, and the solution is represented by cracks defining a rigid macro-block partition of the structure. This directly leads to the formulation of the dual linear problem [49], which represents the discretisation of the minimum of the complementary energy [3]. Its solution provides internal and external forces in equilibrium with the external loads and compatible with the crack pattern solving the primal problem [49]. Therefore, the PRD approach does not require any a priori assumption on mechanisms since fractures and forces are the result of the optimisation problems and depend only on the chosen discretisation [39]. The PRD method has already been used to solve the primal problem in order to find mechanisms in the reference configuration for a wide range of applications: effects of settlement [40,48], cracks due to overloading, such as seismic actions [46], equilibrium of 3D spiral stairs [50], evaluation of the mechanism for the displacement capacity under seismic actions [51], or within an inverse analysis procedure to identify the cause producing a given crack pattern [40,48].

Nonetheless, so far the PRD method has been used only to evaluate the effects of small-displacement fields: this is a necessary but not sufficient step for the assessment of the stability in the deformed configuration or the closeness to the collapse, which can be performed through displacement capacity analyses [30,4,34,35]. To this end, a procedure that takes into account large displacement fields and prevents misleading errors due to the assumption of small-displacement fields is necessary.

The present paper introduces an extension of the PRD method proposing a robust, numerical, displacement-based approach for the application of Limit Analysis to a generic masonry structure undergoing large displacements. The proposed extension allows investigating the effects of large foundation displacements in terms of both cracks/mechanisms and corresponding internal stress states. It is based on the definition of the contact problem assuming gap functions simulating the openings between elements of the discretisation, which, at the same time, preserves the NRNT material assumptions and frames the displacement capacity analysis as a superimposition process of small-displacement fields which results in a sequence of LP problems for NRNT material. For this reason, the internal forces are evaluated

at each step as the dual quantities of the relative displacements, being in this sense compatible with the crack pattern solving the primal problem. With the proposed formulation, new hinges can open during the motion while others can close, also allowing to account for the evolution of both mechanisms and internal forces when the prescribed displacement increases. For these reasons, the PRD method constitutes an efficient and robust way to apply the Heyman model in a broader scenario, not just considering classical stability analyses or small displacement fields, but also taking into account finite displacements.

2. Methods

In this section, we present the piecewise rigid displacement (PRD) method introducing its extension for large displacement problems. Then, we shortly recall the DEM method and describe the combined use of 3DEC with *compas_dem*.

Specifically, in Section 2.1, after recalling how the PRD method frames the search for a solution of the boundary value problem (BVP) for normal, rigid, no-tension (NRNT) materials in a linear programming (LP) problem, we introduce the dual problem and present the approach followed for coupling both LP problems to solve the BVP in the presence of large foundation displacement. In Section 2.2, the main features of *compas_dem,* used in combination with the software 3DEC for benchmarking the PRD analyses, are shortly exposed. Both methods are implemented within the COMPAS framework [52], specifically inside COMPAS Masonry [53], as two distinct packages: *compas_prd* [54] and *compas_dem* [55].

2.1. Piecewise rigid displacement approximation: PRD method

At the beginning of this section, we shortly recall the mathematical framework of the PRD method: for more information, the reader is referred to [42] and for PRD applications of the primal problem to [39].

NRNT material. A 2D masonry structure is modelled as a continuum occupying the region Ω of the Euclidean space $\mathcal{E}^2$. The stress tensor on Ω is $\mathbf{T}$, and $\mathbf{b}$ represents the body load field. Let $\mathbf{u}(\mathbf{x})$ be the displacement field and $\mathbf{E}$ the corresponding infinitesimal strain tensor. The vector $\mathbf{n}$ is the outward normal to the boundary $\partial\Omega$, partitioned into its constrained part $\partial\Omega_D$, where the displacement field $\mathbf{u}(\mathbf{x})$ assumes the value $\bar{\mathbf{u}}$, and into its complementary and loaded part $\partial\Omega_N$ subjected to the applied load $\bar{\mathbf{s}}$ (Fig. 1).

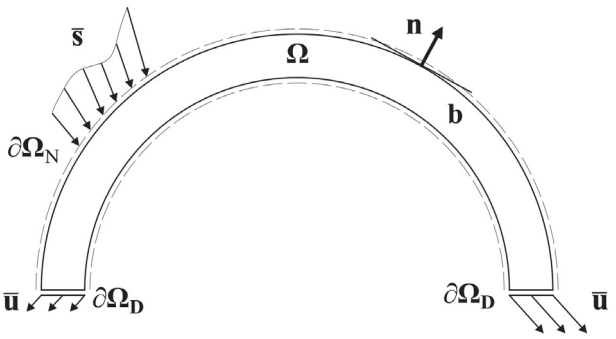

Fig. 1. A two-dimensional continuum occupying a region Ω of the Euclidean space. Load tractions on $\partial\Omega_N$ are represented by $\bar{\mathbf{s}}$ whilst prescribed boundary displacement on $\partial\Omega_D$ by $\bar{\mathbf{u}}$.

The normal, rigid, no-tension (NRNT) material, representing an extension of the Heyman's model into continuum mechanics, is based on the following constitutive relations:

$$\mathbf{T} \in \mathrm{Sym}^-, \quad \mathbf{E} \in \mathrm{Sym}^+, \quad \mathbf{T}\cdot\mathbf{E} = 0 \tag{1}$$

where Sym^- and Sym^+ are the mutual polar cones of semidefinite negative and positive symmetric tensors. These three relations (1) are the necessary assumptions for applying Limit Analysis to masonry structures [40] since they are equivalent to the well-known normality conditions:

$$\mathbf{T} \in \mathrm{Sym}^-, \quad (\mathbf{T}-\mathbf{T}^*)\cdot\mathbf{E} \geq 0, \quad \forall \mathbf{T}^* \in \mathrm{Sym}^-. \tag{2}$$

Boundary value problem. The Boundary Value Problem (BVP) of a continuum composed of a NRNT material subjected to given loads $\bar{\mathbf{s}}$ and displacements $\bar{\mathbf{u}}$ can be summarised with the following relations:

$$\mathbf{E} = \frac{1}{2}\left(\nabla\mathbf{u} + \nabla\mathbf{u}^{\mathrm{T}}\right), \quad \mathbf{E} \in \mathrm{Sym}^+, \quad \mathbf{u} = \bar{\mathbf{u}} \ \text{ on } \partial\Omega_D, \tag{3.1}$$

$$\mathrm{div}\mathbf{T} + \mathbf{b} = \mathbf{0}, \quad \mathbf{T} \in \mathrm{Sym}^-, \quad \mathbf{T}\mathbf{n} = \bar{\mathbf{s}} \ \text{ on } \partial\Omega_N, \tag{3.2}$$

$$\mathbf{T}\cdot\mathbf{E} = 0. \tag{3.3}$$

Thus, the search for a solution of the BVP can be reduced in finding a triplet $(\mathbf{u}, \mathbf{E}(\mathbf{u}), \mathbf{T})$ that at the same time satisfies relations (3). Since the strain tensor $\mathbf{E}$ and stress tensor $\mathbf{T}$ are essentially uncoupled, except for relation (3.3), it is convenient to introduce the following two sets, namely the set of kinematically admissible displacements $\mathcal{K}$ and the set of statically admissible stress $\mathcal{H}$:

$$\mathcal{K} = \left\{\mathbf{u} \in \mathrm{S}/\mathbf{E} = \frac{1}{2}\left(\nabla\mathbf{u} + \nabla\mathbf{u}^{\mathrm{T}}\right) \in \mathrm{Sym}^+ \& \mathbf{u} = \bar{\mathbf{u}} \ \text{ on } \partial\Omega_D\right\}, \tag{4}$$

$$\mathcal{H} = \left\{\mathbf{T} \in \mathrm{S}'/\mathrm{div}\mathbf{T} + \mathbf{b} = \mathbf{0}, \quad \mathbf{T} \in \mathrm{Sym}^-, \quad \mathbf{T}\mathbf{n} = \bar{\mathbf{s}} \ \text{ on } \partial\Omega_N\right\}, \tag{5}$$

where S and S′ are two suitable functionals [56]. Following [42], we call the kinematical problem (KP) the search for an element $\mathbf{u} \in \mathcal{K}$, whilst the equilibrium problem (EP) is the search for an element $\mathbf{T} \in \mathcal{H}$. Two elements, $\mathbf{u} \in \mathcal{K}$ and $\mathbf{T} \in \mathcal{H}$, need to satisfy condition (3.3) to be a solution of the BVP.

Displacement and stress jumps. For NRNT materials, since the strain and stress fields are bounded measures [57–60], they can be decomposed additively into the sum of a regular and a singular part:

$$\mathbf{E} = \mathbf{E}^{\mathrm{r}} + \mathbf{E}^{\mathrm{s}}, \quad \mathbf{T} = \mathbf{T}^{\mathrm{r}} + \mathbf{T}^{\mathrm{s}}. \tag{6}$$

From now on, we will neglect the regular part of the strain: even though this assumption does not stem directly from Heyman's hypothesis, in all his work, Heyman never considered the regular part of the latent strain. For a numerical method and its applications where the regular part of the latent strain $\mathbf{E}^{\mathrm{r}}$ is considered, the reader is referred to [47]. The singular part $\mathbf{T}^{\mathrm{s}}$ is represented by 1D singular stress fields (e.g. thrust lines) while the singular part of the latent strain $\mathbf{E}^{\mathrm{s}}$ by "displacement jumps" along certain lines (e.g. hinges).

Let $\delta(\Gamma)$ be the Dirac delta function having as support a regular curve Γ, whose normal and tangential unit vectors are $\mathbf{n}$ and $\mathbf{t}$. A singular stress field along Γ can be represented as:

$$\mathbf{T}^{\mathrm{s}} = \mathrm{P}\delta(\Gamma)\mathbf{t}\otimes\mathbf{t}, \tag{7}$$

where P represents the magnitude of the concentrated stress and, from Eq. (1), has to be non-positive. On the other hand, a singular strain field $\mathbf{E}^{\mathrm{s}}$ along Γ arises from displacement jumps $[\mathbf{u}]$ across Γ, and thus takes the following form:

$$\mathbf{E} = \mathrm{v}\delta(\Gamma)\mathbf{n}\otimes\mathbf{n} + \frac{1}{2}\mathrm{w}\delta(\Gamma)(\mathbf{t}\otimes\mathbf{n} + \mathbf{n}\otimes\mathbf{t}), \tag{8}$$

where

$$\mathrm{v} = [\mathbf{u}]\cdot\mathbf{n}, \quad \mathrm{w} = [\mathbf{u}]\cdot\mathbf{t}, \tag{9}$$

and since $\mathbf{E} \in \mathrm{Sym}^+$, must satisfy these conditions:

$$\mathrm{v} \geq 0, \quad \mathrm{w} = 0. \tag{10}$$

Primal formulation: minimum of energy criterion. As proved in [40], to solve the BVP problem for NRNT materials, even in the presence of singular fields, an energy criterion can be adopted. Furthermore, assuming only singular strain fields, the solution of the BVP can be obtained as the minimum of the total potential energy of the external loads in a subset $\mathcal{K}_{\mathrm{PRD}}$ of $\mathrm{S}_{\mathrm{PRD}}$ (i.e., the set of small piecewise rigid displacements):

$$\wp(\mathbf{u}^{\circ}) = \min_{\mathbf{u}\in\mathcal{K}_{\mathrm{PRD}}} \wp(\mathbf{u}), \tag{11}$$

where

$$\wp(\mathbf{u}) = -\int_{\partial\Omega_{\mathrm{N}}} \bar{\mathbf{s}}\cdot\mathbf{u}\mathrm{d}s - \int_{\Omega} \mathbf{b}\cdot\mathbf{u}\mathrm{d}a, \tag{12}$$

and with

$$\mathcal{K}_{\mathrm{PRD}} = \left\{\mathbf{u}\in \mathrm{S}_{\mathrm{PRD}}/\mathbf{E} = \frac{1}{2}(\nabla\mathbf{u} + \nabla\mathbf{u}^{\mathrm{T}}) \in \mathrm{Sym}^+ \& \mathbf{u} = \bar{\mathbf{u}} \text{ on } \partial\Omega_{\mathrm{D}}\right\}, \tag{13}$$

the set of kinematically admissible displacements.

PRD method: discretisation of the minimum problem (11). The PRD method represents a numerical procedure for discretising and approximating the minimum problem (11) when the search for a solution is restricted to the set $\mathcal{K}_{\mathrm{PRD}}$. Let the continuum model Ω of Fig. 1 be discretised with M elements (Fig. 2):

$$(\Omega_{\mathrm{i}})_{\mathrm{i}\in\{1,..,\mathrm{M}\}}. \tag{14}$$

The boundary $\partial\Omega_{\mathrm{i}}$ is the union of a finite number of straight lines. A small, piecewise rigid displacement $\mathbf{u} \in \mathrm{S}_{\mathrm{PRD}}$ and defined over the partition (14) can be represented as:

$$\mathbf{u} : \mathbf{x}\in\Omega \rightarrow \begin{cases} \mathbf{u}_1 & \text{if } \mathbf{x}\in\Omega_1 \\ \cdots & \\ \mathbf{u}_{\mathrm{j}} & \text{if } \mathbf{x}\in\Omega_{\mathrm{j}} \\ \cdots & \\ \mathbf{u}_{\mathrm{M}} & \text{if } \mathbf{x}\in\Omega_{\mathrm{M}} \end{cases}, \tag{15}$$

in which $\mathbf{u}_{\mathrm{j}}$ is a small displacement field having Ω_{j} as support. It is well known that each element of (15) is in a one-to-one correspondence with a vector $\mathbf{U} \in \mathbb{R}^{3\mathrm{M}}$ collecting the 3M rigid-body Lagrangian parameters (i.e., for each element of (14), two translations and the rotation around its centre of gravity), namely:

$$\mathbf{u} = \mathbf{u}(\mathbf{U}) \quad \text{with } \mathbf{U}\in\mathbb{R}^{3\mathrm{M}}. \tag{16}$$

Using (16), the total potential energy of the external loads becomes a linear function of $\mathbf{U}$ and can be expressed through a scalar product:

$$\wp(\mathbf{U}) = -\mathbf{c}\cdot\mathbf{U} \quad \text{with } \mathbf{c},\mathbf{U}\in\mathbb{R}^{3\mathrm{M}} \tag{17}$$

where a suitable vector $\mathbf{c} \in \mathbb{R}^{3\mathrm{M}}$ represents the external loads as reduced to two forces and the torque around the centre of gravity of each block. Restrictions (10) need to be enforced on each internal interface (i.e., the interface between two adjacent blocks) of the partition (15) by writing the following relations:

$$\mathrm{v} = [\mathbf{u}]\cdot\mathbf{n} \geq 0, \quad \mathrm{w} = [\mathbf{u}]\cdot\mathbf{t} = 0, \tag{18}$$

on both two endpoints of each internal interface of the partition (15). Referring to Fig. 2b, the physical meaning of restrictions (18) is that the only possible infinitesimal displacement jumps allowed are represented by a complete detachment or by rotations around A or B. Furthermore, they can be collected, using (17), in matrix form:

$$\mathbf{A}_{\mathrm{ub}}^{\mathrm{int}}\mathbf{U} \geq \mathbf{0}, \quad \mathbf{A}_{\mathrm{eq}}^{\mathrm{int}}\mathbf{U} = \mathbf{0}. \tag{19}$$

Similar relations have to be written on all the interfaces lying on the constrained boundary in order to take into account both homogeneous and non-homogeneous conditions, and they are

$$\mathbf{A}_{\mathrm{ub}}^{\mathrm{ext}}\mathbf{U} \geq -\boldsymbol{\delta}_{\mathrm{n}}^{\mathrm{ext}}, \quad \mathbf{A}_{\mathrm{eq}}^{\mathrm{ext}}\mathbf{U} = -\boldsymbol{\delta}_{\mathrm{t}}^{\mathrm{ext}}, \tag{20}$$

where $\boldsymbol{\delta}_{\mathrm{n}}^{\mathrm{ext}}$ [$\boldsymbol{\delta}_{\mathrm{t}}^{\mathrm{ext}}$] is a vector collecting the prescribed displacement $\bar{\mathbf{u}}$ along the normal [tangential] direction on the constrained boundary. For more details on how to enforce the boundary conditions, the reader is referred to [39]. Matrices (19) and (20) can be collected as follows:

$$\mathbf{A}_{\mathrm{ub}}\mathbf{U} \geq -\boldsymbol{\delta}_{\mathrm{n}}, \quad \mathbf{A}_{\mathrm{eq}}\mathbf{U} = -\boldsymbol{\delta}_{\mathrm{t}}, \tag{21}$$

where $\mathbf{A}_{\mathrm{ub}}$ [$\mathbf{A}_{\mathrm{eq}}$] collects vertically the matrices $\mathbf{A}_{\mathrm{ub}}^{\mathrm{int}}$[$\mathbf{A}_{\mathrm{ub}}^{\mathrm{ext}}$] and $\mathbf{A}_{\mathrm{ub}}^{\mathrm{ext}}$ [$\mathbf{A}_{\mathrm{eq}}^{\mathrm{ext}}$], while $\boldsymbol{\delta}_{\mathrm{n}}$ [$\boldsymbol{\delta}_{\mathrm{t}}$] collects the zero vectors arising from (19^1) [(19^2)] and the potential non-zero vectors $\boldsymbol{\delta}_{\mathrm{n}}^{\mathrm{ext}}$ [$\boldsymbol{\delta}_{\mathrm{t}}^{\mathrm{ext}}$] defining the boundary conditions on the constrained part of the structural domain. The set (13) of kinematically admissible displacements becomes

$$\mathbb{K}_{\mathrm{PRD}} = \left\{\mathbf{U}\in\mathbb{R}^{3\mathrm{M}}/\mathbf{A}_{\mathrm{ub}}\mathbf{U} \geq -\boldsymbol{\delta}_{\mathrm{n}}, \mathbf{A}_{\mathrm{eq}}\mathbf{U} = -\boldsymbol{\delta}_{\mathrm{t}}\right\}. \tag{22}$$

If ℓ_{i} [ℓ_{c}] is the number of internal [constrained] interfaces, the dimension of both $\mathbf{A}_{\mathrm{ub}}$ and $\mathbf{A}_{\mathrm{eq}}$ is $2(\ell_{\mathrm{i}} + \ell_{\mathrm{c}}) \times 3\mathrm{M}$. The minimum problem (11) becomes an LP problem:

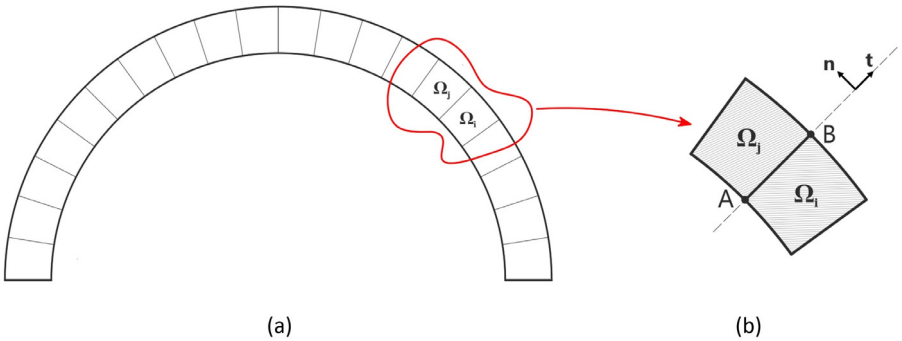

Fig. 2. A possible discretisation of the domain of Fig. 1 (a), and close up of two adjacent blocks (b).

$$\text{minimise} \; -\mathbf{c}\cdot\mathbf{U}$$

$$\text{subject to} \; \mathbf{A}_{\text{ub}}\mathbf{U} \geq -\boldsymbol{\delta}_{\text{n}}, \quad \mathbf{A}_{\text{eq}}\mathbf{U} = -\boldsymbol{\delta}_{\text{t}}, \tag{P}$$

$$\mathbf{U} \in \mathbb{R}^{3\text{M}}.$$

Remark 1. Boundary conditions represented by relations (20) are enforced directly on the interfaces lying on the boundary. Another possible way to write them is to consider external virtual blocks as supports and then to assign prescribed values to the Lagrangian parameters of these supports. In this way, these prescribed values propagate directly to the constrained interface that now can be thought of as "virtual internal interfaces" and thus can be handled as common internal interfaces.

In particular, let Ω_{k} be the element representing the support (Fig. 3), for the interface $\bar{\text{AB}}$, originally lying on the boundary, conditions (18) can be written as:

$$\text{v} = \left(\bar{\mathbf{u}}_{\text{k}} - \mathbf{u}_{\text{i}}\right)\cdot\mathbf{n} \geq 0, \quad \text{w} = \left(\bar{\mathbf{u}}_{\text{k}} - \mathbf{u}_{\text{i}}\right)\cdot\mathbf{t} = 0, \tag{23}$$

where $\bar{\mathbf{u}}_{\text{k}}$ represents the prescribed small rigid displacement of the support. Relations (23) can be rewritten as

$$\mathbf{u}_{\text{i}}\cdot\mathbf{n} \geq -\bar{\mathbf{u}}_{\text{k}}\cdot\mathbf{n}, \quad -\mathbf{u}_{\text{i}}\cdot\mathbf{n} = -\bar{\mathbf{u}}_{\text{k}}\cdot\mathbf{t}, \tag{24}$$

and then collected in the same formal way represented by matrix relations (20) where

$$\delta_{\text{n}}^{\text{ext}} = \bar{\mathbf{u}}_{\text{k}}\cdot\mathbf{n}, \quad \delta_{\text{t}}^{\text{ext}} = \bar{\mathbf{u}}_{\text{k}}\cdot\mathbf{t}, \tag{25}$$

are the known terms. In our opinion, this represents the preferred way to enforce boundary conditions and it will be used later in the numerical applications.

Dual formulation: minimum of complementary energy. Let consider the following linear programming problem:

$$\text{minimise} \; -\mathbf{f}_{\text{n}}\cdot\boldsymbol{\delta}_{\text{n}} - \mathbf{f}_{\text{t}}\cdot\boldsymbol{\delta}_{\text{t}}$$

$$\text{subject to} \; \mathbf{A}_{\text{ub}}^{\text{T}}\mathbf{f}_{\text{n}} + \mathbf{A}_{\text{eq}}^{\text{T}}\mathbf{f}_{\text{t}} = \mathbf{c}, \tag{D}$$

$$\mathbf{f}_{\text{n}} \leq \mathbf{0}, \mathbf{f}_{\text{t}} \in \mathbb{R}^{2(\ell_{\text{i}}+\ell_{\text{c}})},$$

it is easy to see that if $\mathbf{f_n}$ and $\mathbf{f_t}$ are thought of as the dual variables associated with the constraints (20) of the LP problem (P), the new linear programming problem (D) is the dual of (P). Specifically, the dual variables, represented by the vectors $\mathbf{f_n}$ and $\mathbf{f_t}$ and belonging to $\mathbb{R}^{2(\ell_{\text{i}}+\ell_{\text{c}})}$, are the forces dual to the unilateral (18^1) and bilateral (18^2) constraints of the primal problem (P). Moreover, the normal forces $\mathbf{f_n}$ are constrained to be compressive, while the tangential forces $\mathbf{f_t}$ are unconstrained.

The matrix expression in (D) represents exactly the equilibrium of the rigid blocks composing the partition (15); indeed, the equilibrium relation is governed by the transpose of the kinematic matrices of the problem (P) (see also [50]).

The objective function of (D) is the opposite of the work of the dual forces over the generalised displacements. Specifically, the work on the internal boundaries (interfaces between two adjacent blocks) is always zero and only on the constrained boundary it could be non-zero. For this reason, the objective function reduces to the work of the emerging forces (singular stresses) on the constrained boundary over the prescribed boundary displacements, namely: the complementary energy for an NRNT material (i.e., for this material the non-linear part vanishes).

It is worth to point out that, when there is a gap between two adjacent blocks (i.e., the relative displacement is non-zero), the corresponding force has to be zero since there is no contact. On the contrary, if the forces on the boundary of the elements are non-zero, the relative dual displacement has to be zero: in any case, the objective function reduces to the complementary energy.

In this sense, the solution of the dual problem (D) allows finding internal (between blocks) and external forces (on the constrained boundary) in an assembly of rigid block acting unilaterally without sliding. Furthermore, if the prescribed boundary displacements are zero, the solution represents one of the possible admissible stress states in equilibrium with the given loads [49]. Problem (D) is the discretised form of the following problem: "Find a minimiser $\mathbf{T}^0 \in \mathcal{H}_{\text{PRD}}$ of the complementary energy:

$$\wp_{\text{c}}(\mathbf{T}) = -\int_{\partial\Omega_{\text{D}}} \text{s}(\mathbf{T})\cdot\bar{\mathbf{u}}\,\text{ds}, \tag{26}$$

where $\mathbf{s}(\mathbf{T})$ is the trace of the stress tensor on the constrained boundary $\partial\Omega_{\text{D}}$ and $\mathcal{H}_{\text{PRD}}$ the space of the emerging stresses (i.e., Dirac delta distributions) at the boundary of each element of the partition (15). In particular, the discretised set $\mathbb{H}_{\text{PRD}}$ of admissible stress states (a subset of $\mathcal{H}_{\text{PRD}}$) is

$$\mathbb{H}_{\text{PRD}} = \left\{\mathbf{f} = [\mathbf{f_n}, \mathbf{f_t}] \in \mathbb{R}^{4(\ell_{\text{i}}+\ell_{\text{c}})} / \mathbf{A}_{\text{ub}}^{\text{T}}\mathbf{f}_{\text{n}} + \mathbf{A}_{\text{eq}}^{\text{T}}\mathbf{f}_{\text{t}} = \mathbf{c}, \quad \mathbf{f}_{\text{n}} \leq \mathbf{0}, \quad \mathbf{f}_{\text{t}} \in \mathbb{R}^{2(\ell_{\text{i}}+\ell_{\text{c}})}\right\}. \tag{27}$$

For more details about the emerging stresses and their use, and why this generalisation is needed for NRNT materials, the reader is referred to [42,40]. The first proof and an application of the use of the minimum of the complementary energy for NRNT material can be traced back in [3].

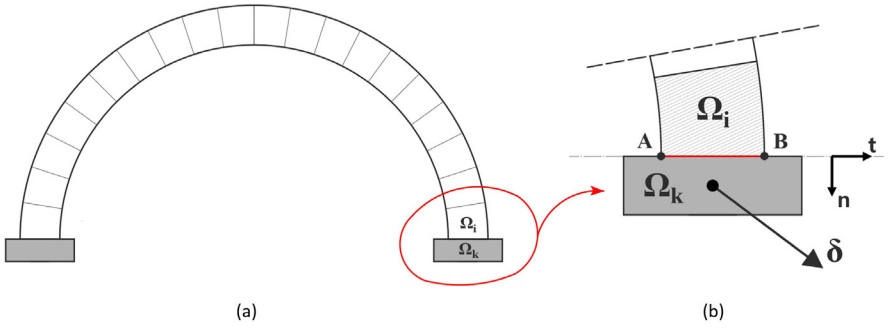

Fig. 3. To simulate external boundary conditions, virtual blocks (in grey) can be added as supports (a). The original constrained interface becomes a regular internal interface (b).

Approximation of large displacement fields. For NRNT materials, the natural way to numerically account for large displacement fields (e.g. large support displacements) is to recursively apply the PRD method on the deformed configuration in a step-by-step procedure as a sequence of standard LP problems. To this aim, as shown in [51], finite rigid displacement fields can be approximated by considering small-displacement fields in a superimposition process. It is worth noting that in [51] the PRD was applied just to select the initial rigid macroblock partition of the domain which, after that, was considered fixed during the analysis. To approximate large displacement fields, and thus potential openings during the motion, relations (18), defining a perfect, continuous contact on an interface between two adjacent blocks, have to be properly rewritten to consider potential cracks.

Indeed, once the primal problem has been solved for the first time, the original interface $\bar{AB}$ (Fig. 4a) can exhibit a displacement jump (i.e. crack). For the sake of simplicity, let's imagine the case when a hinge forms (Fig. 4b): point B splits into two distinct points, B_i and B_j, and thus the blocks Ω_i and Ω_j are touching only in A. Let d_B be the measure of the gap between B_i and B_j and $\mathbf{d}_B$ the corresponding unit vector. Relations (18) still hold for A, namely:

$$v_A = [\mathbf{u}]_A \cdot \mathbf{n} \geq 0, \quad w_A = [\mathbf{u}]_A \cdot \mathbf{t} = 0, \tag{28}$$

but, only a unilateral relation ensuring a no-penetration condition with an initial gap d_B has to be written for B, that is:

$$v_B = [\mathbf{u}]_B \cdot \mathbf{d}_B \geq -d_B. \tag{29}$$

Eq. (28) enforce the NRNT material restrictions on the deformed configuration (as assumed in the past by several authors, see for instance [4,32,35]), while Eq. (29) ensures that there is not a material overlapping. In particular, once the primal and dual problems have been solved for the first time, the geometry is updated using the solution of the primal problem (P). For each step, on the new, deformed geometry, all the contact restrictions defining the set of admissible displacements are properly updated taking into account the presence of crack through relations (28) and (29). The external loads are re-evaluated on the deformed geometry and, consequently, a new objective function of the primal problem (P) is considered. With this approach, a new primal problem (P) is formulated. It preserves the same form (P), while the dual problem (D) is always obtained as the dual of the updated problem (P). It is worth noting that during the motion, with the present formulation, as it will be clearly shown in the applications, a fracture (e.g. hinge) can close, restoring the continuity along with the original interface. In particular, if during the motion Eq. (29) is satisfied as equality, the NRNT material restriction will be restored and taken again into account through relations represented by Eq. (28), that is through relations (18) written on the update configuration. Thus, with the present formulation since a hinge can open and close during the motion, the mechanism can change according to the new boundary conditions, and consequently, the internal forces are always compatible with the mechanism solving the primal. The procedure takes place until the total potential energy governing the primal problem is not bounded from below anymore: the structure becomes unstable and collapses.

Remark 2. Despite force-based approaches, which can model masonry as an assembly of rigid blocks [16,17] also considering large displacement fields [19], the PRD method represents a numerical displacement-based approach to solve the boundary value problem for a continuum composed of NRNT material. Indeed, the main idea behind the development of this numerical method is to handle the displacements as primal data and to catch, as a result of the analysis, the subdivision of the structural domain into rigid macroblocks, in particular when settlements take place or also when the structure is subjected to overloading or to severe seismic actions [46]. In this sense, the PRD method is a displacement-based approach which allows to computationally apply standard limit analysis à la Heyman to generic masonry structures without any a priori assumption on the mechanism and, to directly handle as primal data the non-homogeneous boundary conditions. Moreover, since the PRD approach allows to couple two dual-energy criteria, that is the minimum of both total potential energy and complementary energy, the dual variables are represented by the internal forces which are obtained always as dual quantities of the relative displacements on the interfaces defined by a given partition and arising from the piecewise displacement field solving the primal problem. The extension of the PRD method proposed in the current paper allows at the same time preserving the NRNT material assumptions and framing the displacement capacity analysis as a superimposition process of small-displacement fields which results in a sequence of LP problems. For this reason, the internal forces are in each step evaluated as the dual quantities of the relative displacements, being in this sense compatible with the crack pattern solving the primal problem.

2.2. Discrete element modelling and compas_dem

Discrete Element Modelling (DEM) is a method able to analyse structures composed of multiple bodies. Cundall [61] first developed this approach at the beginning of the 1970s for modelling granular materials, and in the last decades, it has also been applied to masonry constructions [62–64]. In this paper, the DEM software 3DEC by Itasca [65] has been used. In DEM, the model is composed

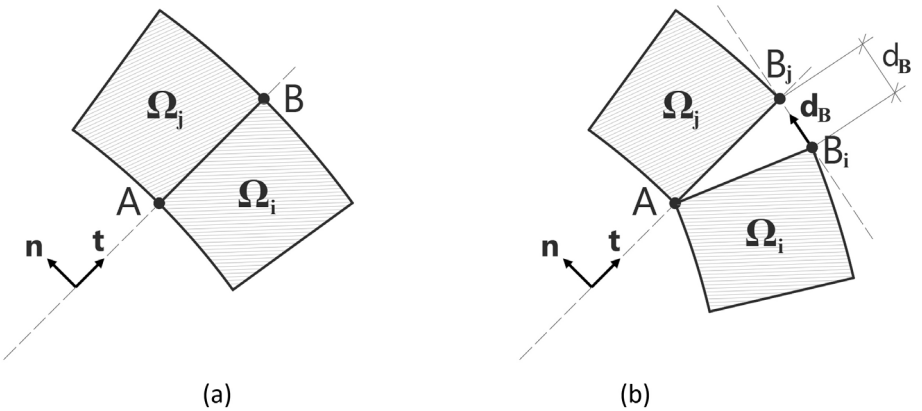

Fig. 4. Two adjacent blocks in a perfect contact condition (a). Two blocks hinged around one corner (b).

of separated blocks interacting with each other at the interfaces. The blocks can be considered rigid or deformable, and Mohr-Coulomb failure criteria can be used to model the joints:

$$\tau = \sigma \tan(\varphi) + c, \tag{30}$$

where τ is the shear strength, σ is the normal stress, φ is the friction angle and c the cohesion.

Moreover, the blocks can move and deform independently with respect to each other; they can get completely separate, and they can form new contacts with other blocks during the analysis.

Since the blocks can be considered rigid and the contact interfaces with no tensile strength, this method is suitable for the investigation of the behaviour of unreinforced masonry structures. The unilateral behaviour of masonry structures can be well-described, and Heyman's assumptions [2] can be approximated, making the application of the Limit Analysis possible. Another advantage of using rigid blocks interacting with no tensile strength is the reduction of the number of mechanical parameters required in the analysis. In this case, the analysis only requires the density of the material, its friction angle and the joint stiffness, a parameter specific to 3DEC to calculate the contact forces between the blocks. If the tensile strength at the joints is neglected, also the cohesion in the Mohr-Coulomb failure criteria does not need to be taken into account. There is no need for other mechanical parameters, which, especially for historic masonry structures, are based on uncertainty, or they are impossible to predict. The motion of the blocks in the DEM method is described by Newton's second law and solved numerically by the central difference method with respect to a scalar parameter (e.g. time). The position of the blocks during the calculation is updated step by step. Two different kinds of analyses are possible, static and dynamic, and both solved with explicit numerical algorithms.

The relation between blocks is described by the contact forces between the blocks' interfaces. Each contact force is a function of the block displacement at that point, which in turn depends on the values of the joint stiffness. Two values of the joint stiffness have to be defined: the normal joint stiffness and shear joint stiffness. These values control the elastic deformation of the block assembly at the joints and are used by 3DEC to calculate the contact forces between the blocks' interfaces. Physically, the two joint stiffnesses control, respectively, the penetration and the sliding between blocks. Both phenomena should be avoided during the simulation of unreinforced masonry structures as rigid blocks, and for this reason, a high value for the joint stiffnesses should be used. On the other hand, as shown by [9,13], the values of the joint stiffness could be reduced to significantly decrease the calculation time without influencing the results of the analysis a lot. The two joint-stiffness values of the joint stiffness are calculated according to [10]:

$$J_{kn} = E/h_{block}, \quad J_{ks} = G/h_{block} \tag{31}$$

where J_{kn} is the normal joint stiffness, E is the Young's modulus of the material, and h_{block} is the block's height. For the evaluation of the joint shear stiffness, the E has been replaced by G (shear modulus) evaluated as:

$$G = E/2(1+\nu). \tag{32}$$

where ν is the Poisson's coefficient considered equal to 0.2. With this method, several aspects can be studied: displacement capacity, collapse, three-dimensional behaviour, stability, the effects of different load cases (e.g. point load, linear, distributed, with gradient), settlements, and any variation in the boundary conditions. A key aspect of using the DEM method is the discretisation of the model. To perform a three-dimensional analysis, the model needs to be discretised in a meaningful way, either using the actual stereotomy or a representation of it. In this paper, the DEM analyses have been conducted using *compas_dem* [55], a Python-based, general-purpose computational tool for working with assemblies that can use the software 3DEC in the background extending its modelling possibilities and the elaboration of the results. To achieve the objectives of this paper related to the numerical modelling of cracks in typical architectural elements of a Gothic cathedral, *compas_dem* has been used to calculate the resultant contact forces at interfaces between the blocks and to visualise the flow of forces.

At each vertex of the interfaces, 3DEC computes normal and shear forces and visualises them as contour plot over the interface (see, e.g. the contour plot of the normal stresses in Fig. 5b). By taking all interface forces provided by 3DEC, *compas_dem* computes the normal and shear resultants on each interface (Fig. 5e) and the interface resultant also (Fig. 5d), allowing, in this sense, a better understanding of the mechanical behaviour. Thanks to this elaboration and consequent visualisation, it is possible to clearly identify the changes in the internal forces due to different boundary conditions. Furthermore, the study of both flow of forces and point of application of the resultants makes the opening of cracks in the structure easily readable. Since the proposed analyses are planar, we will show just the 2D projection of the 3DEC.

3. A benchmark case: pointed arch

In this section, we look, as a benchmark case, to the study of a pointed arch on spreading support, referring to physical tests presented in [66] and briefly summarised in Section 3.1. A PRD analysis of the same arch geometry using *compas_prd* [54] is shown in Section 3.2. The results of the PRD analysis are further validated with the ones obtained with *compas_dem* and 3DEC (Section 3.3). The comparison in terms of crack pattern, internal singular stress state and displacement capacity is reported and discussed in Section 3.4.

The aim is twofold: firstly, use both the physical tests and the 3DEC results for benchmarking the PRD analysis and, secondly, use this simple numerical example as a pilot case to introduce the next application based on a cross-section of a Gothic cathedral.

3.1. Physical test

The benchmark case, here proposed, has been selected from [66,67] where the behaviour of the Gothic arch had been intensively and parametrically explored based on both analytical formulations and test cases. Particularly, in the experimental campaign in [66], several tests on pointed arches, constructed of cast concrete voussoirs with no mortar between the blocks, were carried out paying particular attention to the effects of support displacements in terms of both crack pattern and displacement capacity. To describe the geometry of a pointed arch, we follow the same notations used in [67] (Fig. 6a):

- R_{circ} is the radius of the circular arch measured to the centreline of the arch;
- R_{point} is the radius of the pointed arch measured to the centreline of the arch;
- e eccentricity of the centre of the arch with respect to the axis of symmetry;
- t is the thickness of the arch; and,
- α is the angle of embrace.

The geometry of the pointed arch, composed of 14 voussoirs with mass density $\rho = 1800$ kg/m^3 and here proposed as a benchmark, is defined by the following values: $R_{circ} = 1$ m, $t/R_{circ} = 0.12$, $e/R_{circ} = 0$ and $\alpha = 150^{\circ}$ and a span of 0.95 m. The arch was tested by horizontally moving the right support outwards until collapse.

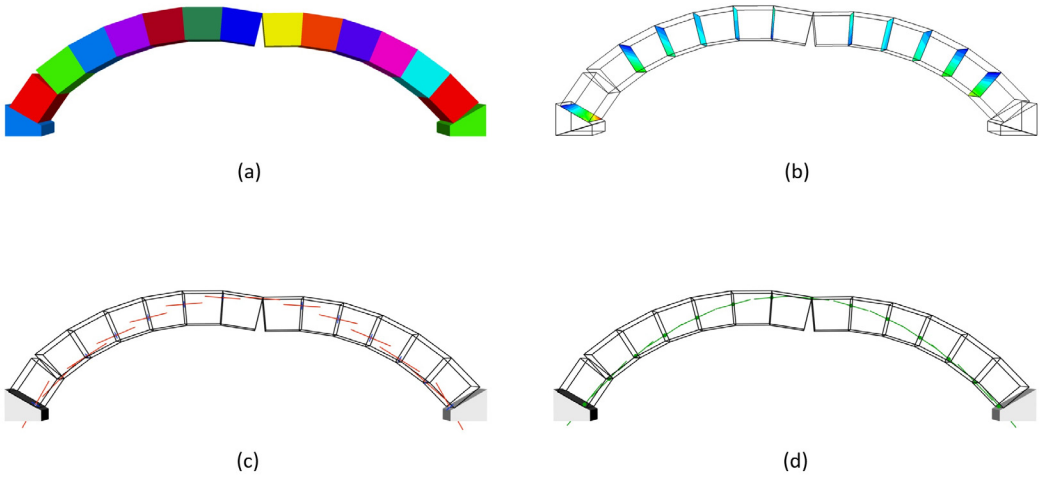

Fig. 5. Typical 3DEC analysis output of a circular arch subjected to horizontal, outward support movements: deformed configuration (a), contour plot of the normal stresses (b). Visualisation of the interface forces provided by *compas_dem*: normal (red lines) and shear forces (blue lines) (c), resultant forces (in green) in (d). (For interpretation of the references to colour in this figure legend, the reader is referred to the web version of this article.)

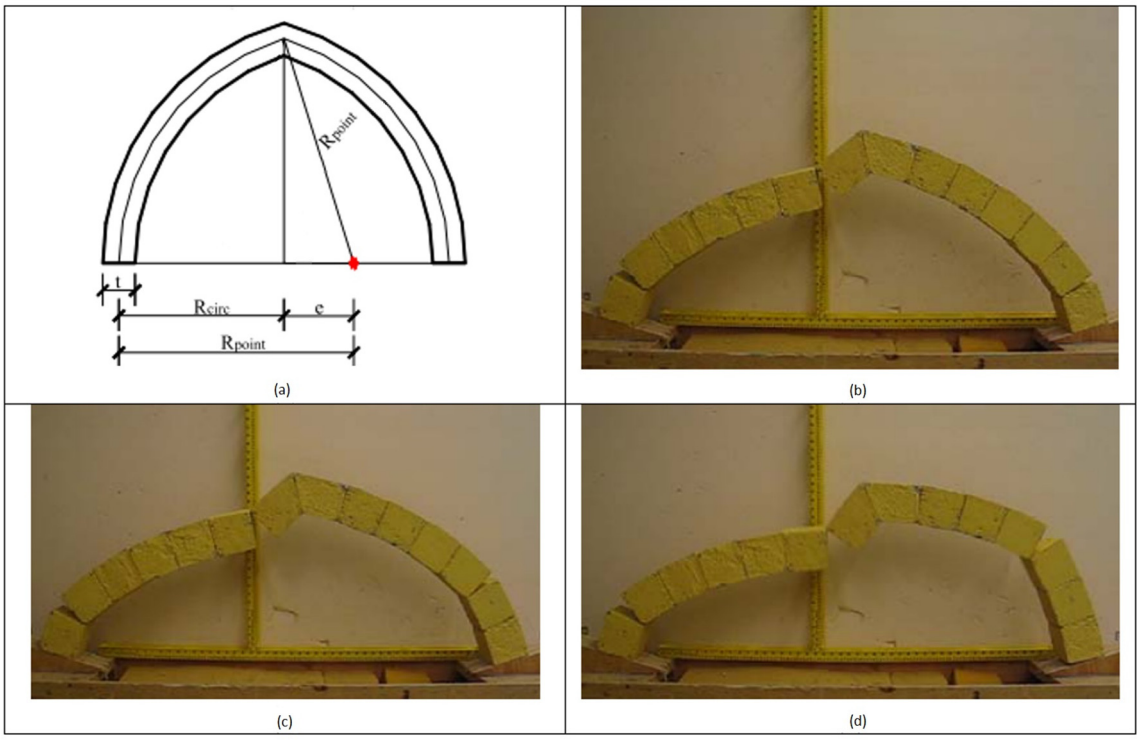

Fig. 6. Notations used in [67] and to parametrically describe the shape of a pointed arch (a); images from [66] of the physical test conducted on the pointed arch subjected to the spreading of the right support whose geometry is defined by $R_{circ} = 1$ m, $t/R_{circ} = 0.12$, $e/R_{circ} = 0$ and $\alpha = 150^{\circ}$ and a span of 0.95 m (b–d).

In Fig. 6b–d, the images of the physical tests catching the last steps before collapse are reported. In particular, when the right support started moving, a three-hinge mechanism formed (Fig. 6b) and it remained fixed until the arch approached the maximum allowable displacement: in this condition, the hinge on the right part moved suddenly up to the crown (Fig. 6c–d), and a fourth hinge formed (Fig. 6d) between the wooden base and the right support causing the collapse. In [66], the maximum allowable displacement was evaluated as the one corresponding to the situation depicted in Fig. 6c, and estimated as 245 mm. Furthermore, the author also conducted a numerical analysis based on an equilibrium approach predicting a maximum displacement of 290 mm.

3.2. PRD analysis

The same pointed arch shown in Section 3.1 is here modelled and analysed with the PRD method using *compas_prd*. Two further blocks are added as supports (highlighted in grey in Fig. 7a, see Remark 1). Firstly, the pointed arch has been analysed in its undeformed configuration, considering homogeneous boundary condi-

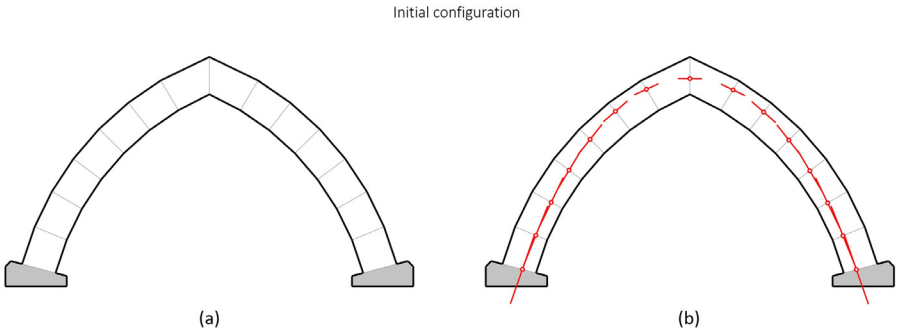

Fig. 7. The pointed arch is discretised into 14 blocks and two further blocks (highlighted in grey) are added as supports: (a). Representation of the solutions of the primal (P) and dual (D) problems for the initial, perfect configuration, that is when the arch is not subjected to foundation displacements: (b).

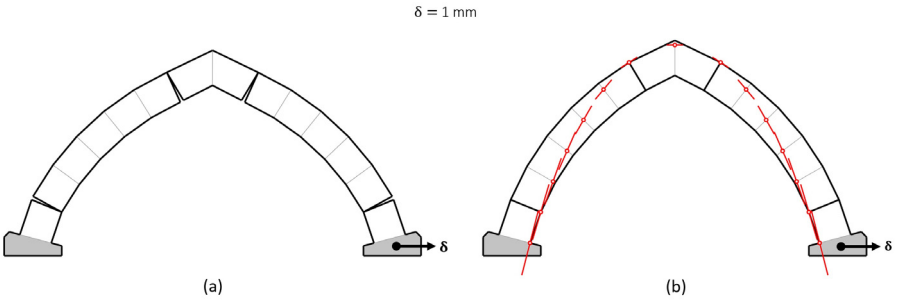

Fig. 8. The pointed arch, subjected to an outward displacement δ of 1 mm. The solution of the primal problem (P) scaled up by a factor of 10 (a): only the interfaces where cracks occur are labelled with bold black lines. The forces, solving the dual problem (D) are represented through their resultants: (b).

tions. In Fig. 7, the results of the primal and dual problems are shown: no hinges form and the resultant forces are everywhere lying within the structural geometry, representing a safe and one of the admissible stress states. Both LP problems have been solved with CVXPY [68] choosing MOSEK [69] as a solver. The total computational time to initialise the model and to define and solve both LP problems is about 0.03 s with an Intel® Core™ i7-8850H.

Then, the pointed arch has been analysed after imposing an outward horizontal displacement on the right support. In Fig. 8, the solutions of both primal (P) and dual (D) problems are depicted considering an outward horizontal displacement δ of 1 mm. Also in this case, the computational time needed by *compas_prd* to initialise the model and to define and solve both problems is 0.028 s. Specifically, the solution of the primal problem returns four symmetrical hinges, representing singular strain fields on the interfaces between adjacent blocks where cracks appear. The solution of the dual problem returns forces between blocks which are reduced to their resultants, as shown in Fig. 8b. These forces are compatible with the cracks found with the primal problem: they pass exactly through the centre of rotation defined by the hinges. It is worth to point out that the thrusts on the supports are very close to the internal points of the interface without touching them.

Then, the arch is analysed increasing the displacement of the right support in steps of 1 mm until it collapses. Both the primal problem (P) and the dual (D) are at/for each step written on the deformed configuration. The total computational time needed for the displacement capacity analysis to define and solve both problems is 5.514 s.

In Fig. 9, the solutions of both the LP problems are depicted on the deformed configurations referring to six different steps. Particularly, just after the support displacement increases and reaches the value of 2 mm (Fig. 9a), the right hinge near the crown (Fig. 9b–c) closes while the left one remains open: the arch becomes a three-hinge stable mechanism. The mechanism qualitatively remains the same until the displacement reaches the value of 261 mm (Fig. 9c) when the hinge near to the right support moves up: the arch is still stable in this configuration (Fig. 9d). The maximum allowable displacement for which the structure is still stable is 278 mm (Fig. 9e). When the support displacement is 279 mm, the right hinge moves suddenly up and the arch reaches an unstable configuration and starts collapsing (Fig. 9f).

Remark 3. The four-hinge mechanism of Fig. 8a is perfectly symmetric and differs from the mechanisms (Fig. 6b) of the physical tests. The reason is simple: because of the perfect and symmetric geometry, both the mechanisms are equivalent, at the same energy level, and thus both are possible solutions of the BVP. Nonetheless, when the displacement increases (Fig. 9), one of the two central hinges (Fig. 8a) closes and the other one remains open (Fig. 9b).

3.3. DEM analysis

In this section, the displacement capacity analysis is carried out on the same pointed arch using *compas_dem* with 3DEC as solver, and applying an incremental displacement of 1 mm per step. The value of the Young's modulus adopted is 30GPa.

Since 3DEC allows to consider the friction angle of the material as a parameter, three different analyses have been performed using three different friction angles: 35°, 50° and 90°. In 3DEC, the displacement is applied by assigning a velocity field to the supports. After every step, the velocity was set to 0 and the calculation of the out-of-balance forces was run for three seconds, to check if the structure was still in equilibrium in the deformed configuration. The three analyses performed, assuming different values of the friction

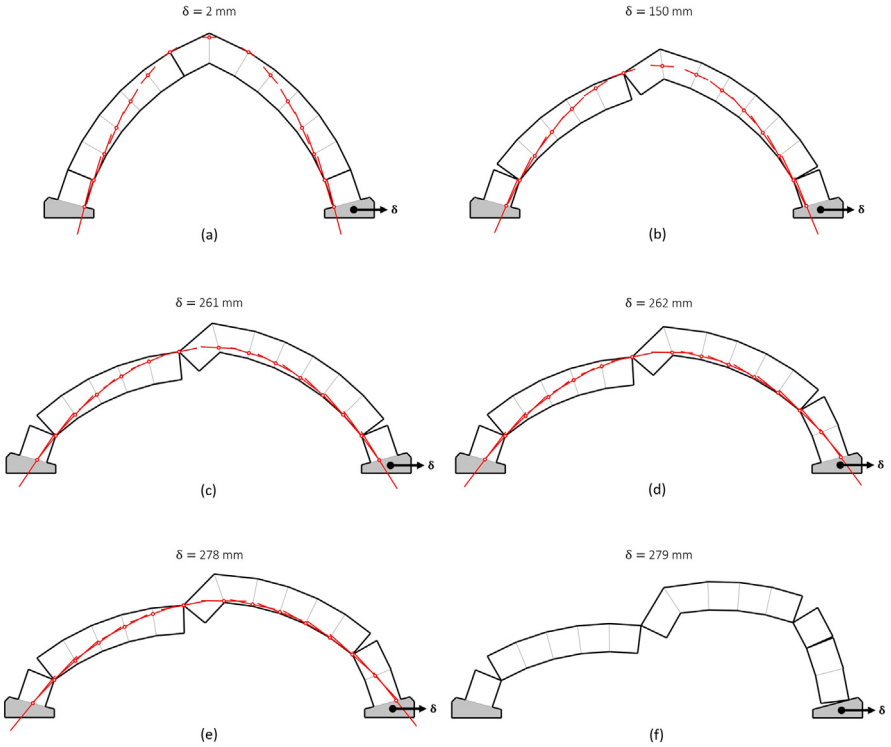

Fig. 9. Solutions of both the linear and dual problems on the deformed configuration: geometric configurations, crack patterns and resultant forces for $\delta = 2$ mm (a), $\delta = 150$ mm (b), $\delta = 261$ mm (c), $\delta = 262$ mm (d), 278 mm (e) and for the unstable configuration corresponding to $\delta = 279$ mm (d).

angle, showed the same behaviour in terms of cracks, forces and displacement capacity. In what follows, we report and describe the results obtained with a friction angle of 35°. After the first step (Fig. 10b), a three-hinge mechanism forms. It remains fixed (Fig. 10c–d) until the displacement reaches the value of 259 mm when the hinge near to the left support moves up (Fig. 10e). The last step before the collapse, where 3DEC could still find an equilibrium state of the structure, is for a displacement of 274 mm (Fig. 10f). The calculation with 3DEC, reducing the joint stiffnesses by 10 to increase the solving time, takes about 4200 s, so over an hour, with an Intel® Core™ i7-6820HQ.

3.4. Discussion

In this section, the PRD analysis is compared with the results of the physical tests and with the ones obtained from 3DEC and elaborated with *compas_dem*. First, we have to point out that the experimental tests differ from the theoretical model in some points. The blocks considered in the numerical applications have perfect geometry. Furthermore, in the PRD analysis, two blocks can exhibit a relative rotation or a complete detachment but sliding phenomena are not taken into account. On the other hand, real blocks are affected by geometrical imperfections, which reflects into non-smooth contacts over the interfaces. A first consequence of the imperfections is that even though a physical test is designed on a perfect ideal symmetric geometry, the actual geometry is never symmetric. Secondly, due to the imperfections, the displacement capacity can be slightly different between the numerical and the physical tests [13].

The PRD analysis (Fig. 9) reproduced the same behaviour in term of crack pattern and hinge positions, shown in the physical test (Fig. 6). The ultimate stable displacement predicted with the PRD analysis is 278 mm (Fig. 9e), while in the physical was estimated as 245 mm corresponding to Fig. 6c. In [66] the author proposed a numerical displacement capacity analysis following a continuous equilibrium approach on the deformed geometry predicting a maximum displacement of 290 mm: the PRD analysis is less conservative since it is based on discretised geometry representing the actual one, and can predict the change in the mechanism.

Referring to the 3DEC results, we have to point out that the mechanism found is specular to the one obtained with *compas_prd* and the one found during the physical test: even this solution is admissible on a perfect and symmetric geometry (Remark 3).

Even if the mechanism is specular, starting from a very small displacement (2 mm) both PRD and 3DEC provide the same qualitative three-hinges mechanism, which remains the same until the displacement of the right support reaches the value of 259 mm. From this value on, the left hinge in 3DEC starts moving up, while this behaviour (the right hinge) happens in PRD starting from a value of 262 mm. The displacement capacity predicted by the PRD analysis is 278 mm, similar but a little bit larger than the one obtained by 3DEC (274 mm).

Assuming the thrust on the supports as a measure of the internal stress states, in Fig. 11 the curves representing the plot of the horizontal and vertical components of the thrust as a function of the support displacement are depicted. These curves are non-linear and coincident until a displacement of 259 mm. When the hinges move up (259 mm for 3DEC and 262 for PRD) there is a jump: in between these two values the slopes of the curves is the same and from 262 mm on, all curves return to be coincident until 274 mm (maximum allowable displacement predicted by 3DEC). The solution obtained with the DEM analysis is essentially coincident with the one from PRD.

Remark 4. Looking at the curves (Fig. 11) related to the PRD analyses, it should be pointed out that whenever a hinge forms or moves in another position, the curves exhibit a jump. Particularly, when the arch starts moving, three hinges form and the thrust (see, for instance, the horizontal components of the thrust in Fig. 11)

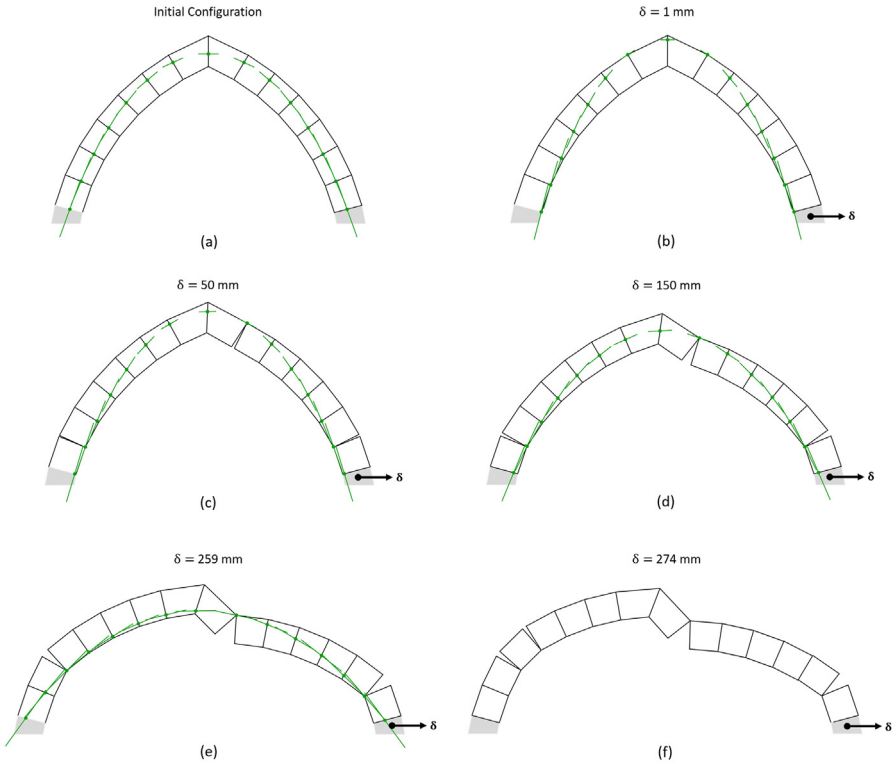

Fig. 10. 3DEC results of the displacement capacity analysis visualised through *compas_dem*: resultant contact forces on the undeformed configuration (a), crack pattern and resultant forces for $\delta = 1$ mm (b), $\delta = 50$ mm (c), $\delta = 150$ mm (d), $\delta = 259$ mm (e), $\delta = 274$ mm (f).

suddenly drops. This is a peculiar behaviour of rigid blocks structures with unilateral contacts, such as masonry structures: they reach a new configuration, often statically determined, and the forces between blocks vary to catch a new equilibrium state (which is unique for the statically determined part of the structure).

4. Gothic cathedral subject to a foundation displacement

The case study here presented regards the analysis of the cross-section of a Gothic cathedral. The assessment of such complex structures is a hard task since several structural elements are working together and cannot be decoupled in the analysis. Furthermore, even though such cathedrals were built following geometric rules rather than mechanical knowledge, they are still around showing remarkable adaptability to different boundary conditions. In the last decades, many studies have been conducted on the structural behaviour of Gothic cathedrals considering distinct structural aspects and using different approaches. In [70] and [71], photoelasticity has been applied regarding different load cases (e.g. wind loads) and to explain existing crack patterns. In [72,73] the finite element method (FEM) has been adopted to analyse the effect of dead, lateral and seismic loads, and the structural behaviour during the construction phase. Both the photoelasticity and FEM approaches cannot well reproduce the unilateral behaviour of the masonry as also stated in [74] or in [75] and in [1] where limit analysis (LA) has been applied and recognised as one of the most suitable methods for masonry structures. A common way to approach through LA this problem is to use thrust line anal-

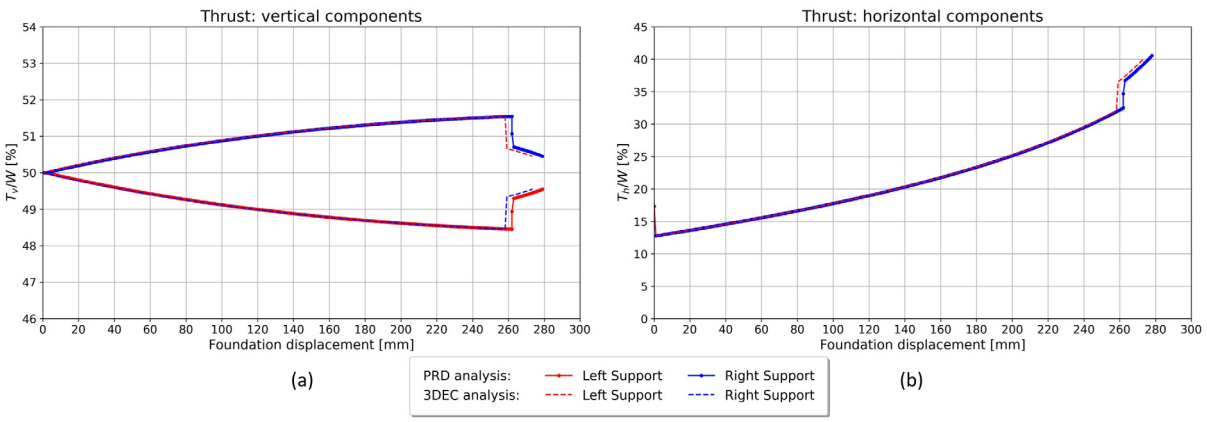

Fig. 11. Comparison between the results from the PRD analysis, using *compas_prd*, and 3DEC: vertical (a) and horizontal (b) components of the thrust on the supports.

yses (TLAs), based on the slicing technique [76,77]. In [78], a kinematic approach has been used to assess the safety under wind loads but selecting a small number of mechanisms in advance. In [79], a study on the role of pinnacles of the Amiens cathedral has been conducted using different approaches. These papers prove that there is still a lack of a numerical model able to find cracks, mechanisms and forces and which can also account for the effect of (even large) foundation displacements. With the following numerical case study, we want to show how the PRD method can bridge this gap, applying limit analysis and selecting the solution from a space composed of ∞^{3M} possible mechanisms (defined by Eq. (14)).

In this section, using the PRD method, we perform a displacement capacity analysis investigating the evolution of both the crack pattern and the corresponding stress state within the structure. In particular, the aim is twofold: showing the abilities of the PRD method in such analyses and showing the ductility of Gothic structures under foundation displacements. The same analysis is performed with 3DEC and the results are compared.

The structural cross-section considered is an approximation of the cross-section of the Amiens Cathedral (Fig. 12). The objective here is not aiming to assess it but to show an application based on real proportions and structural elements of a Gothic structure. Fig. 12 shows the plan and the 3D scheme taken from [80].

4.1. Model geometry and discretisation

The PRD analysis has been conducted using *compas_prd*, which in its current implementation is designed for planar, 2.5D analysis, that is: the analysis is planar but non-uniform, symmetrical orthogonal depths can be considered. In Fig. 13a, the main dimensions of the cross-section considered in the analysis are reported. The structure is symmetric, the height of the central nave is 42.00 m, the height of the aisle is 19.00 m and the distance between two consecutive cross-sections is 7.30 m.

We have to point out that since the analysis is planar, the cross vaults on the central nave and on the aisles are modelled as pointed arches with an orthogonal depth of 7.30 m, so the 3D behaviour of these vaults is neglected, but such an approximation allows to take into account the effects due to the self-weight and to the thrusts exerted. Furthermore, since the considered cross-section is not external, the thrusts of the cross vaults are acting in a vertical plane, making that approximation less distant from the actual working state. In Fig. 13b, the dimensions of the depth of the structural elements are reported.

Acquiring the actual stereotomy of a structure is all too often impossible thus, discretising the structure into sub-elements (e.g. blocks) is a complex task demanding a good knowledge of the mechanical behaviour of such structures. The geometry of the cross-section shown in Fig. 13a, has been discretised following reasonable rules: the vertical elements have been cut using horizontal planes whilst curved elements, such as the pointed arches and the flying buttresses, with joints perpendicular to the curvature (Remark 5). In Fig. 14a, the discretisation adopted for both the PRD and 3DEC analyses is depicted: the structural geometry is partitioned into 276 rigid blocks and four further blocks are added as supports. In Fig. 14b**, a 3D** view of the geometry, including the supports, is reported.

Remark 5. One of Heyman's hypothesis regards the no-sliding condition. The reason why Heyman enunciated this assumption, behind the need for proving the two basic theorems of limit analysis, stays in the fact that master masons built structures following rules to prevent sliding phenomena. These ancient rules, coded with the term "regola dell'arte" [24], are based on a clever arrangement of the stones composing the structure. In particular, in masonry walls, on the horizontal planes, the sliding is prevented by high values of the compressive forces while, on the vertical plane, where the compressive force is very low, by a particular arrangement of the bricks through interlocking; furthermore, on curved elements, the stones are arranged with joints orthogonal to the curvature. It is worth noting that while the sliding between real blocks is a negligible and thus a secondary effect for several 2D structures (the ones conceived following particular construction details), in general, mechanisms involving 3D curved structures cannot form without overcoming friction, that is without sliding between real blocks, which is needed to accommodate those movements (the reader is referred to [9] or to [50] where a 3D spiral stair is analysed through the PRD approach allowing for small sliding effects). The Heyman theory can be framed as a "metamodel" where the representative element is not the brick. Furthermore, it is worth to point out that the word "stereotomy" (from the greek Στερεός "solid" e Τομή "cut") denotes a complex "art", but it is much more than an art: it is a science requiring a deep knowledge and connection between three-dimensional geometry and stone cutting to have a flow of forces as perpendicular as possible to the joints [22].

4.2. PRD analysis

The Gothic cathedral of Fig. 14a is here analysed considering a foundation displacement δ below the third pillar (starting from the left side). As external load, only the self-weight due to a uniform distribution of mass density ($\rho = 1800$ kg/m^3) is considered. After performing an analysis in the initial configuration, we increase the displacement δ in steps of 1 cm each until the structure collapses. The total computational time needed for this displacement capacity analysis to define and solve both the primal (P) and dual (D) problems is about 30 s with an Intel® Core™ i7-8850H.

In Fig. 15, the solutions related to six different values of the displacement field are shown: both the primal problem (P) and its dual (D) are solved in the deformed configuration. The solution of the primal problem returns the new configuration of the structure and the cracks, whilst the solution of the dual problem returns internal and external forces (i.e. emerging singular stresses) in equilibrium with the given external loads and acting on the boundary of each element. Particularly, the tolerance assumed to detect a crack (e.g. opening) is 0.01 cm: in Fig. 15 all interfaces exhibiting a crack are identified with bold, black lines.

Furthermore, from Fig. 15, one can see that the forces are compatible with the crack pattern solving the primal problem: indeed, if a hinge forms the force goes through the relative centre of rotation. In Fig. 15a the forces in the initial configuration are depicted: they are everywhere within the structural geometry, and they flow down almost vertically along the central pillars. It is worth to point out that, as in the spirit of the limit analysis, they represent only one of the infinite admissible stress states. Starting from a value of the displacement of 1 cm (Fig. 15b), the flow of forces changes radically: a hinge forms in between the support and the third pillar (the one affected by the foundation displacement) and the flow of forces, at least for the right side of the cathedral, is less vertically than before.

From Fig. 15c–f it can be seen that the mechanism is roughly the same even though the location of the hinges change a little (see for instance the two flying buttresses on the right side). Specifically, the mechanism corresponding to δ = 1 cm (Fig. 15b) remains the same (e.g. Fig. 15c) until the displacement reaches the value of 59 cm: starting from this value the position of the hinges on the flying buttresses change (Fig. 15d).

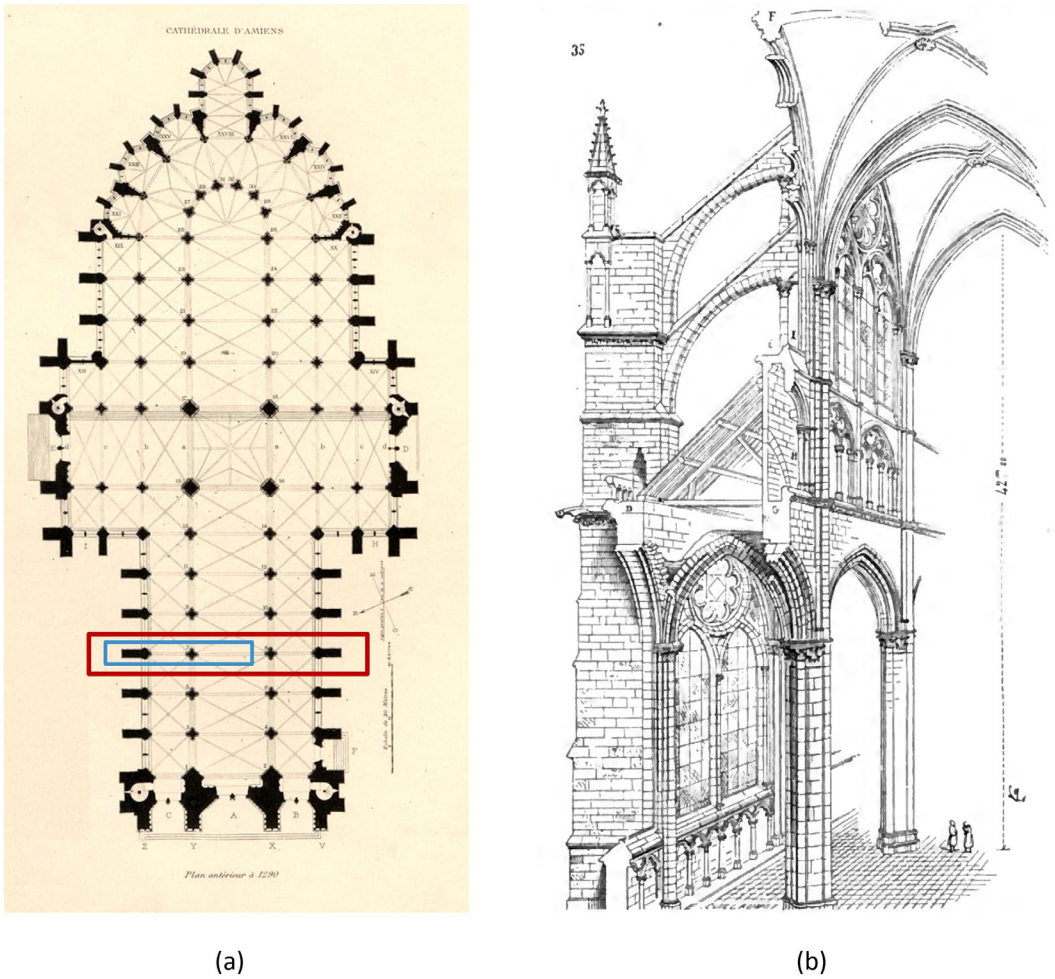

Fig. 12. Draws of Amiens cathedral from [80]: plan (a) and three-dimensional scheme (b). The cross-section considered in the analysis is denoted by the red rectangle in (a) while the blue rectangle in (a) highlights the structural elements depicted in (b). The depth between two consecutive cross-sections is 7.30 m. (For interpretation of the references to colour in this figure legend, the reader is referred to the web version of this article.)

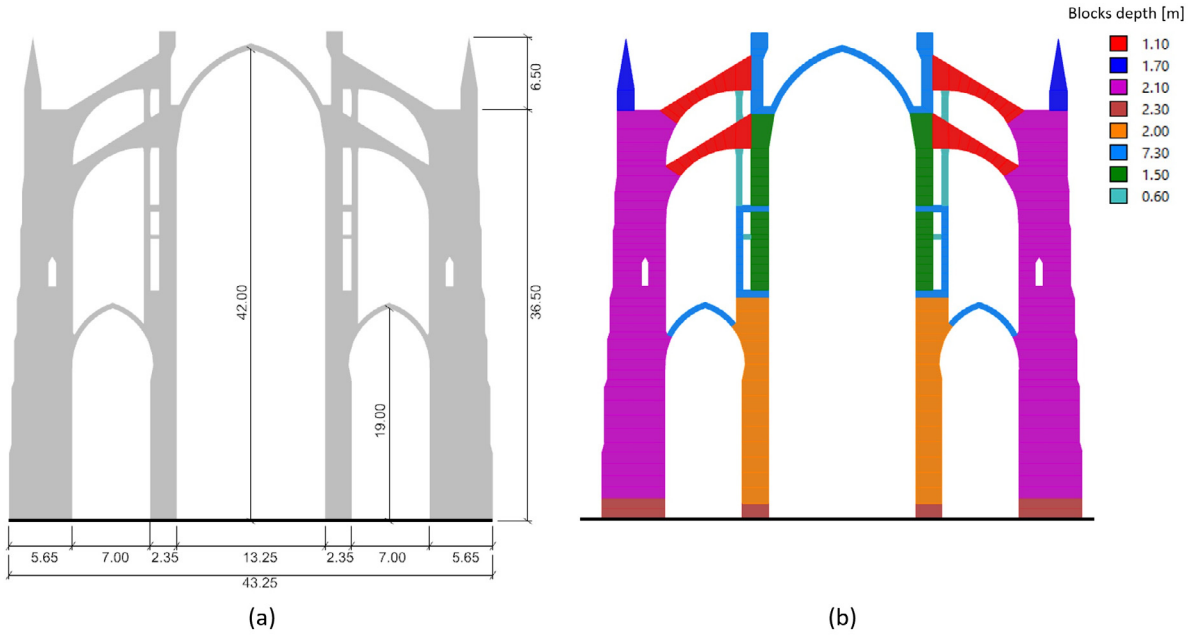

Fig. 13. Main dimensions of the cross-section (a) and orthogonal depth of the structural elements (b).

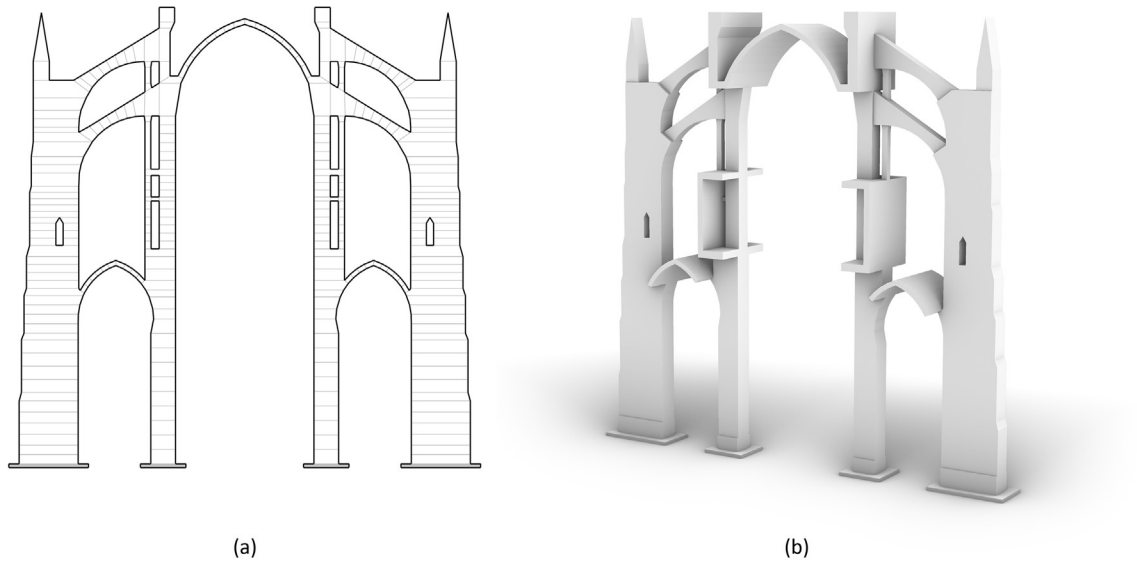

Fig. 14. The cross-section shown in Fig. 13 has been partitioned into 276 rigid blocks and four blocks (in grey) have been added as supports (a). 3D view of the geometry (b).

A similar change occurs when the displacement reaches the value of 146 cm: the mechanism switches from the one depicted in Fig. 15e to the one reported in Fig. 15f, which corresponds to the last stable configuration before the collapse. Therefore, the ultimate allowable displacement is 180 cm, and the corresponding crack pattern is depicted in Fig. 16a. Fig. 16b–c illustrate the evolution of the collapse mechanism reached when the displacement δ equals 181 cm: the central nave arch starts collapsing (Fig. 16b), the third pillar moves a little on the left side and consequently, the flying buttresses become unstable (Fig. 16c).

Moreover, looking at Fig. 15c–f, one can see that when the structure is approaching the collapse, the flow of forces in the upper part of the right buttress becomes more and more vertical, suggesting that the flying buttresses are losing any chance to reach an equilibrium state due to the increasing, relative outward displacements of their boundaries. In this situation, the total potential energy, that is the objective function of the primal problem, is not bounded from below anymore as shown in Fig. 17a.

In the next Sections 4.4 and 5, we report the values of the thrusts exerted by the main structural elements and the values of the displacement of some control points (CPs) located over the structure. For the location of the CPs, for the structural elements considered and for the sign of the thrusts, the reader is referred to Fig. 17b.

4.3. DEM analysis

Here, the same displacement capacity analysis of the Gothic cathedral model is performed with 3DEC assuming the same incremental vertical displacement δ in steps of 1 cm as done for the PRD analysis, and a friction angle equals to 35°. In the initial configuration under zero given displacements, the flow of forces appears everywhere within the structure (Fig. 18a). As soon as the displacement δ below the third pillar starts, hinges and cracks start forming, and the flow of forces changes accordingly (Fig. 18b). The crack pattern evolves (Fig. 18c–e) as in the analysis with *compas_prd*, showing the formation of a hinge at the base of the third pillar and hinges in the flying buttresses. The positions of the hinges in the flying buttresses slightly change when δ is 82 cm and when δ is 125 cm. The maximum allowable displacement is 177 cm, since the collapse happened for δ equals to 178 cm, starting from the central nave vault (Fig. 18f). The calculation with 3DEC takes about 10800 s, about 3 h, with an Intel® Core™ i7-6820HQ without reducing the joint stiffnesses.

4.4. Comparison

In this section, the results of the PRD displacement capacity analysis performed on the Gothic cathedral model are shortly compared with the ones obtained with 3DEC and elaborated with *compas_dem*.

The displacement capacity with the PRD method is 180 cm, almost equal to the 177 cm obtained with the DEM analysis. Even the evolution of the mechanisms and of the crack pattern is similar. The only slight differences are related to when the changes in the mechanisms occur. In particular, the detected collapse mechanism is exactly the same starting from the central nave arch and then involving the flying buttresses. In Fig. 19, the curves represent the vertical and horizontal components of the thrust exerted on the supports evaluated with both methods.

The solution in terms of thrusts is similar with some slight differences. The global trend is the same: all the curves have the same slopes. Moreover, the value of the thrust on the third and fourth pillars are very similar, while some differences are recognisable only on the values concerning the first and second pillars. It is interesting to see that these two pillars are not involved in the mechanism, and thus the left part of the structure remains statically indeterminate. In that part, the results obtained with the PRD analysis represent, as in the spirit of limit analysis, just one of the infinite admissible stress states.

Furthermore, it has been shown that the computational time needed by the PRD analyses is of a few seconds also to perform a complete displacement capacity analysis. This depends on the fact that the minimum energy criteria are framed as LP problems, and currently, there are many available algorithms (such as the interior-point ones) which can allow fast computational solving even in presence of very large problems. In Table 1, the time needed to initialize the PRD model, to solve a single PRD analysis and to perform an entire PRD displacement capacity analysis is reported and as well as the one required by 3DEC. Referring to the PRD analyses, the LP problems have been solved with CVXPY [68] choosing MOSEK [69] as a solver with an Intel® Core™ i7-8850H. The 3DEC analyses, based on explicit dynamics, have been conducted with an Intel® Core™ i7-6820HQ. Looking at the 3rd and

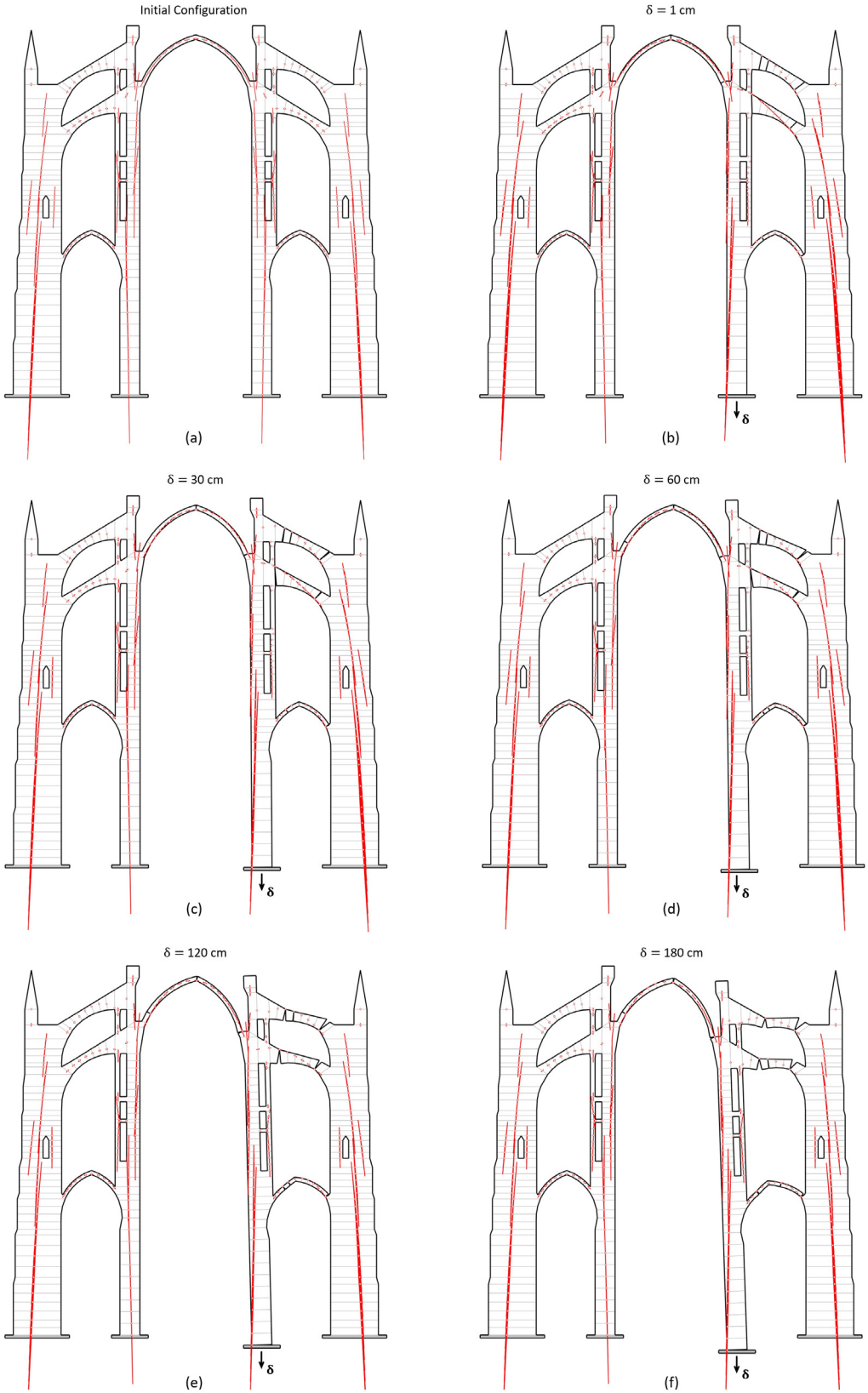

Fig. 15. Representation of the solutions of both the linear and the dual problems. Geometric configurations, cracks pattern (interfaces labelled in bold black) and resultant forces for: initial undeformed configuration (a), $\delta = 1$ cm (b), $\delta = 30$ cm (c), $\delta = 60$ cm (d), $\delta = 120$ cm (d), $\delta = 180$ cm (e).

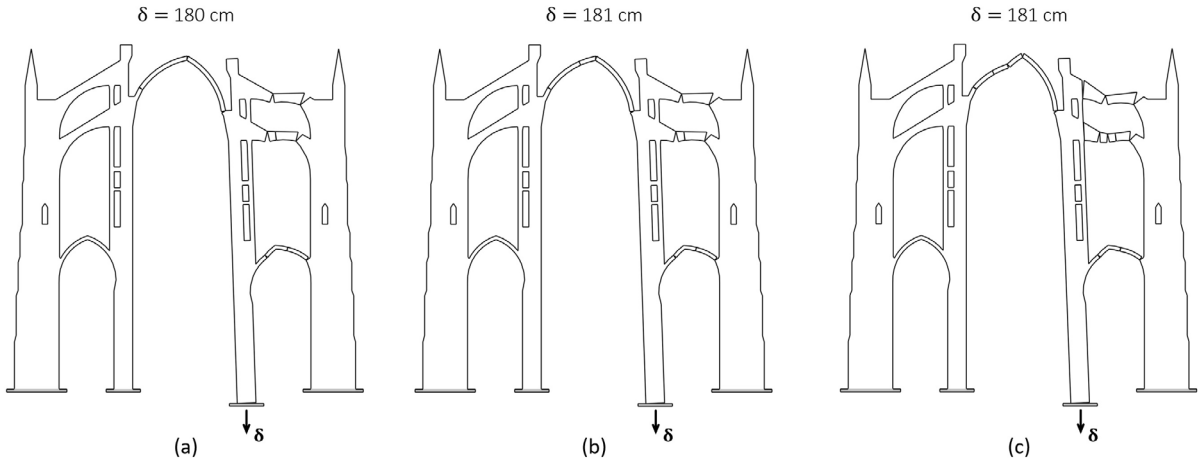

Fig. 16. The ultimate allowable displacement is 180 cm (a). For δ = 181 cm the central nave arch equals becomes unstable (b), the third pillar moves on the left side suddenly and the flying buttresses lose any chance to reach a new equilibrium state (c).

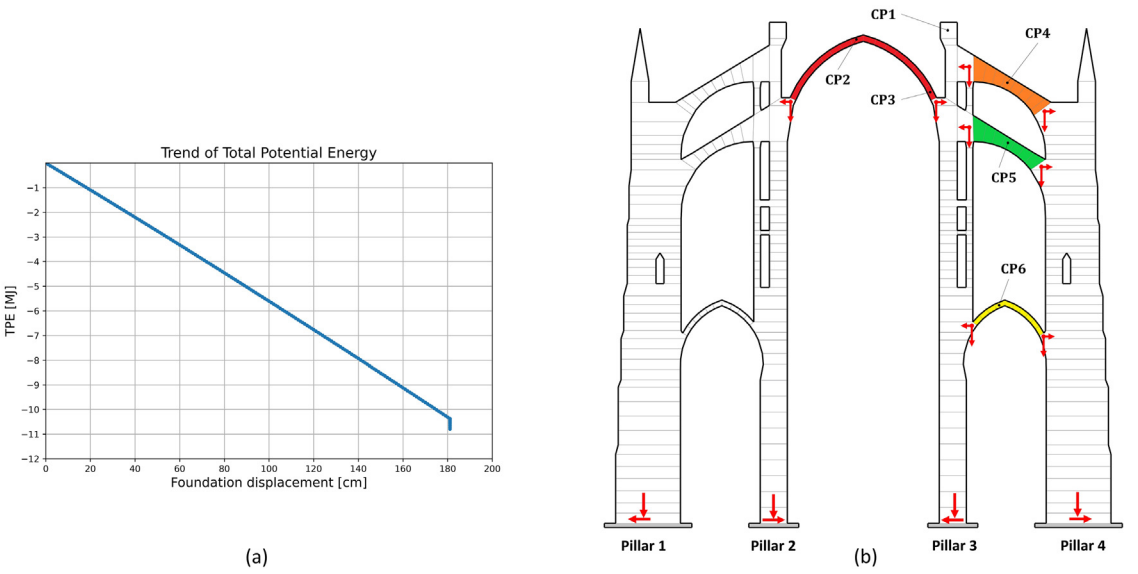

Fig. 17. In (a) the plot of the total potential energy (TPE) as a function of the value of the vertical displacement: when the structure becomes unstable ($\delta = 181$ cm) the energy is not bounded from below anymore. (b): arrows defining positive values of the thrusts exerted by some structural elements: central nave arch (red), upper flying buttress (orange), lower flying buttress (green), aisle arch (yellow); localisation of control points (CPs). (For interpretation of the references to colour in this figure legend, the reader is referred to the web version of this article.)

4th columns of Table 1, the net time required for solving just the LP problems corresponds to the difference among the 4th and 3rd columns. Moreover, during the PRD displacement capacity analyses, the model does not need to be initialised anymore, since as exposed in Section 2.2, the LP problems are simply updated. It can be seen that the time required, when compared to 3DEC, is much less. Since in both cases, the PRD analyses are in good agreement with the results obtained with 3DEC, the fast computational solving opens up the possibility, not just to perform small-displacement inverse analyses [40], but also to take into account, when needed, large-displacement inverse analyses.

Remark 6. Looking at both the PRD and 3DEC analyses, it can be observed that the third pillar of the Gothic cathedral is moving downward monolithically until the collapse. Moreover, the pillar, hinged on its left-bottom part, shows a slight, increasing rotation around that corner, but its configuration is stable until the upper part of the cathedral starts collapsing. Specifically, looking at the PRD displacement capacity analysis, the fact that the third pillar behaves as monolithic is just a result of the analysis. If different forces/boundary conditions would have been present, the analysis could have returned e.g. a different location of the hinge/hinges or a loss of its local stability. Indeed, to illustrate how the PRD approach can catch different behaviour due to various boundary conditions, in what follows we propose a PRD displacement capacity analysis of the cross-section of the Gothic cathedral coupling the effect of the vertical settlement with the rotation of the support. In particular, we assume that in each step the support of the third pillar is subjected to a vertical displacement of 0.01 m and a counterclockwise rotation of 0.001 rad around its centroid. The PRD displacement capacity analysis returns a maximum allowable displacement equal to 60 cm. The computational time required for each step of this new analysis is the same needed by the previous analysis (see Table 1) being the matrices defining the

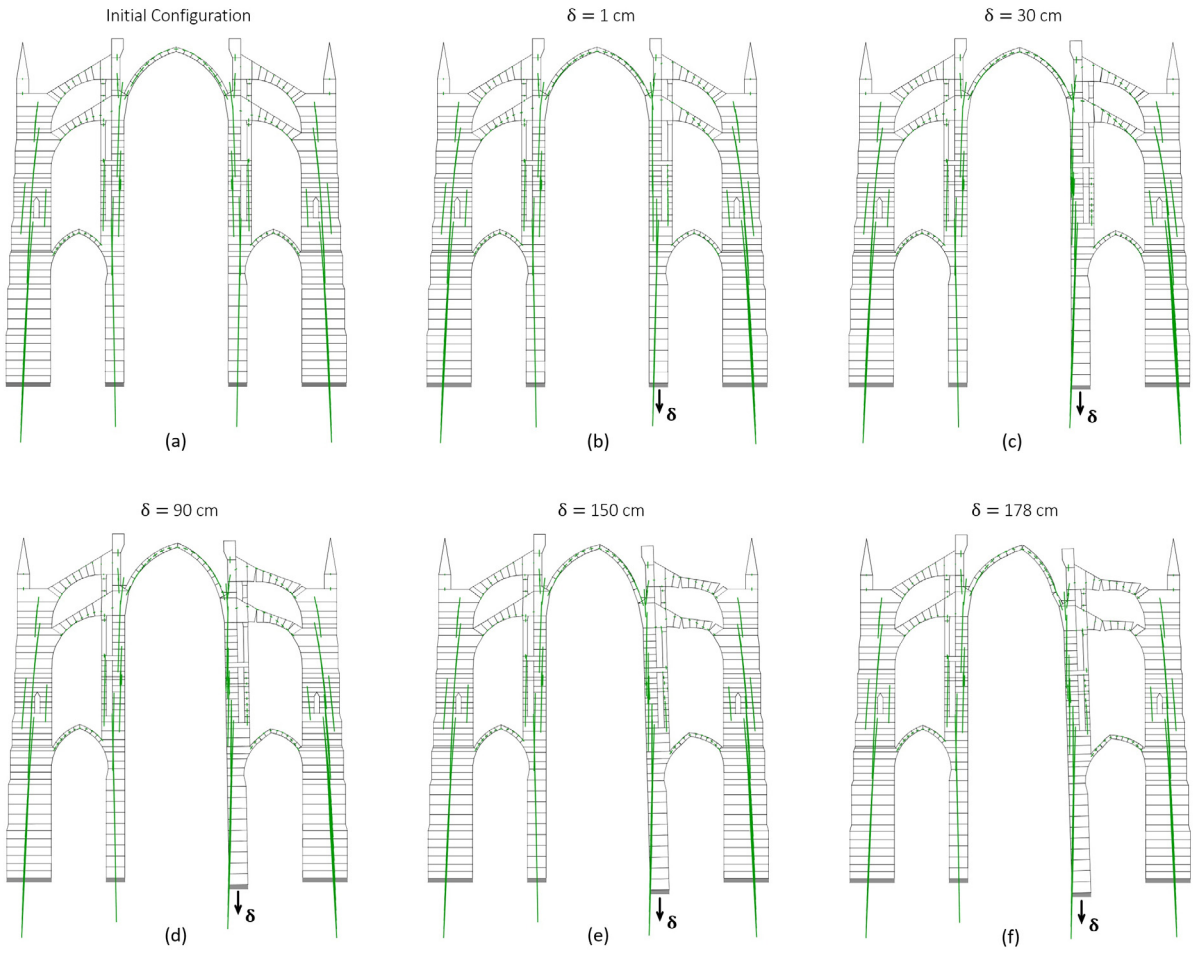

Fig. 18. Representation of the 3DEC solutions through *compas_dem* for the initial undeformed configuration (a), $\delta = 1$ cm (b), $\delta = 30$ cm (c), $\delta = 90$ cm (d), $\delta = 150$ cm (e) and for the unstable configuration corresponding to $\delta = 178$ cm (f).

LP problems the same. Even in this case, the analysis has been benchmarked with 3DEC through the use of compas_dem and, the maximum displacement obtained is 58 cm.

The results in terms of displacements, cracks and internal stress states obtained from the PRD analysis and corresponding to three different boundary conditions are reported in Fig. 20a–c. As main outcome of this analysis, it can be noted that the mechanism changes and the third pillars shows a horizontal hinge and thus is not behaving monolithically anymore. In particular, Fig. 20c illustrates the last stable configuration obtained via the PRD analysis, while Fig. 20d shows the last stable configuration obtained via *compas_dem*, corresponding to a vertical foundation displacement equal to 58 cm: the detected collapse mechanism is exactly the same. Looking at the horizontal and vertical thrust exerted by the third pillar, Fig. 20e depicts the comparison amongst the PRD and 3DEC. It shows a good agreement between both approaches.

From a numerical perspective, this further investigation shows how the PRD approach can easily handle different boundary conditions. From a mechanical perspective, if the vertical settlement is coupled with a rotation, the mechanical behaviour of the structure changes. Indeed, in this case, the additional boundary condition influences the behaviour of the structure for small foundation displacements (e.g. the initial mechanism can be completely different) and the stability fors finite displacements (the maximum allowable displacement in this last analysis is lower).

The PRD approach can be applied to different mechanical problems and with different boundary conditions. One of the key features is that, as stated in the **Introduction**, it does not require any a priori assumption on mechanisms since fractures and forces are the results of the optimisation problems and depend only on the chosen discretisation (the reader is referred to [39,40,46,48] or for further benchmarks to [39]). Indeed, the space of the mechanism is defined by the number M of the element of the structural partition. Specifically, using the PRD method, the solution is selected in a space composed of ∞^{3M} possible mechanisms: in the case of the Gothic arch, the dimension is 14 while in the case of the Gothic cathedral the dimension is 276. The mechanism solving the minimum problems depends on the load and on the boundary conditions. In this sense, thanks to the two variational formulations on which is based, it represents a displacement-based approach that performs limit analysis à la Heyman selecting the mechanism solving the primal problem among a wide spectrum of admissible mechanisms and thus does not depend on a particular, apriori choice of the qualitative crack patterns. For this reason, it can be applied to masonry structures such as the ones reported in [5,6,30,33] by accurately identifying in each specific case, as a function of the construction details (Remark 5), the resisting structural model. E.g., if the aim is to assess masonry arch bridges, a conservative approach commonly adopted when standard Limit Analysis methods are applied to look for the load-bearing capacity or seismic assessment, is to model the structure through arches over piers and to opportunely take into account the backfill/spandrels through proper load distributions or additional resisting structures (for more details, the reader is referred

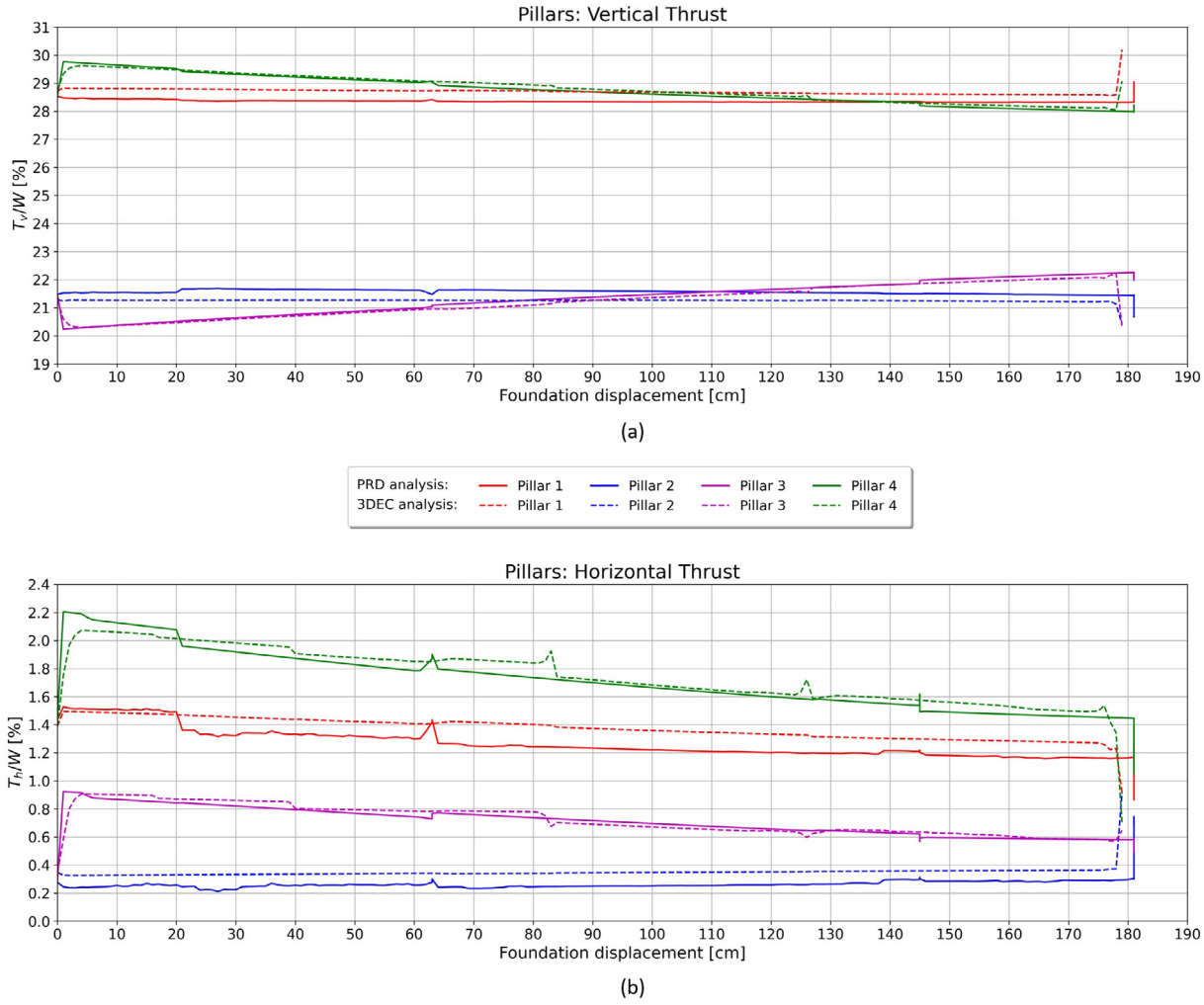

Fig. 19. Thrust on the supports obtained with the PRD and 3DEC analyses: vertical (a) and horizontal (b) components dimensionless with respect to the total weight of the structure.

Table 1
Computational time required for PRD and 3DEC analyses. δ_{max}^{PRD} and δ_{max}^{3DEC} represent the maximum allowable displacements for PRD and 3DEC analyses, respectively.

	Elements [–]	Step [cm]	Initialise PRD model [s]	PRD single analysis [s]	PRD displ. cap. analysis [s]	δ_{max}^{PRD} [cm]	3DEC displ. cap. analysis [s]	δ_{max}^{3DEC} [cm]
Gothic arch	14	0.1	0.004	0.028	5.514	27,8	4200	27,4
Gothic cathedral	276	1	0.205	0.369	28.958	180	10800	177

to [81] and references therein). In this light, the PRD approach offers practitioners and scholars one more option which can integrate other models in the assessment of historic masonry structures, particularly when subjected to foundation displacements.

5. Discussion

In this section, referring to the Gothic cathedral application, we discuss the results obtained with the PRD method in-depth to show how it provides a new computational way for applying Limit Analysis on complex and generic planar masonry structures subjected to large foundation displacements. In Section 4.2, a PRD analysis, coupling the primal (P) and dual (D) problems, of a two-dimensional section of a Gothic cathedral, based on the gross dimensions of Amiens, has been performed. Firstly, the cathedral has been analysed in the initial (perfect) configuration to assess if the structure is stable or not, and then, in the deformed configuration obtained in a step-by-step procedure by prescribing an increasing foundation displacement below the third pillar until the structure reaches an unstable configuration (Fig. 15). In Section 4.4, the results have been compared with the one obtained with 3DEC, showing good agreement in terms of crack patterns, mechanisms and resultant forces.

The solution in the reference configuration (Fig. 15a) shows that the cathedral is stable since the total potential energy corresponding to the solution of the primal problem (P) is bounded from below and the dual problem (D) provides an internal stress state lying everywhere within the geometry. It is worth to point out that, as in the spirit of Limit Analysis, they represent only one of the infinite admissible stress states, as indeed the complementary energy is constant and equals zero. After assessing the initial stability, a displacement capacity analysis has been performed and the maximum allowable displacement is estimated as 180 cm: when δ is equal to 181 cm the total potential energy is not bounded from

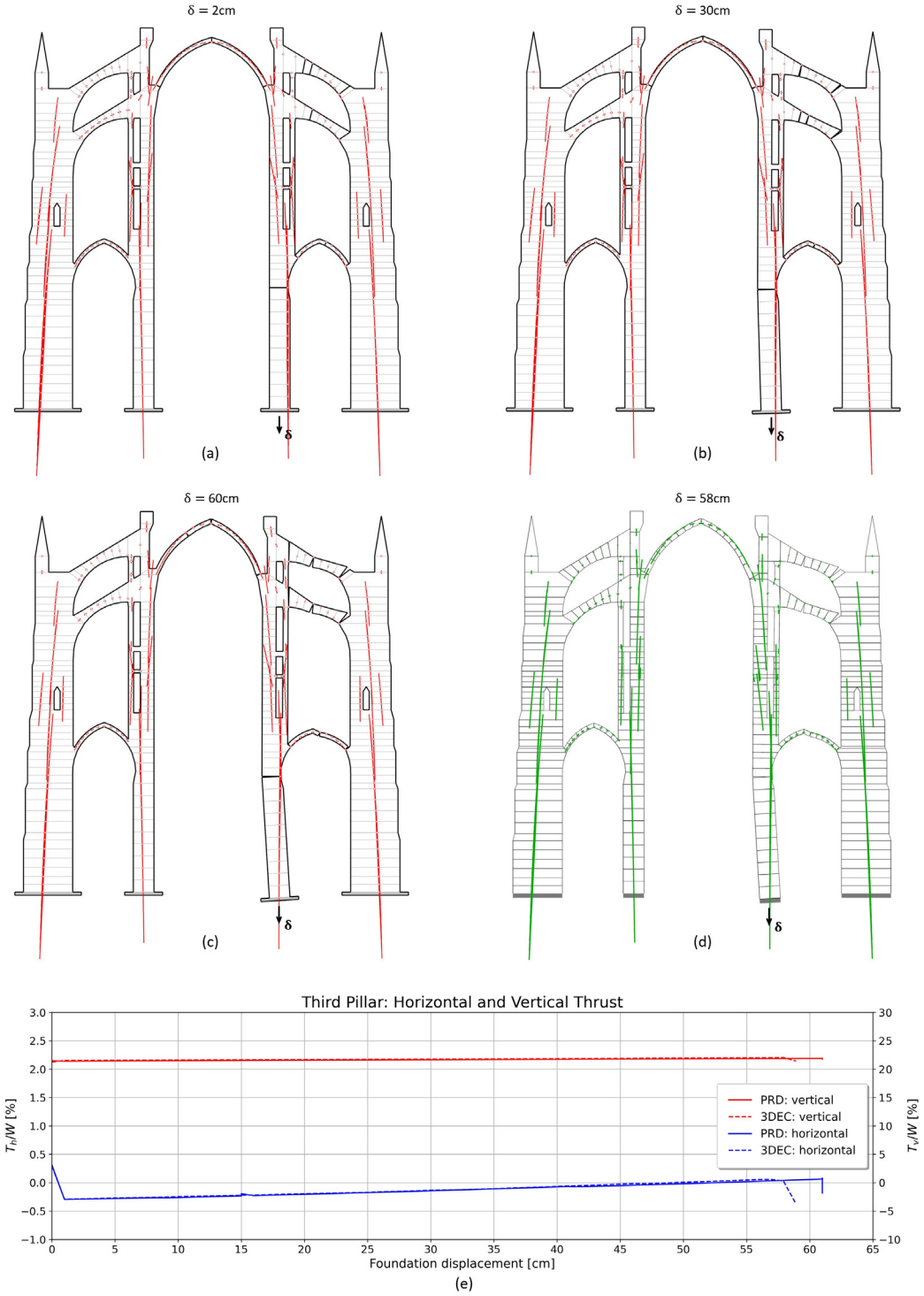

Fig. 20. In (a–c), PRD displacement capacity analysis of the cross-section of the Gothic cathedral subjected to settlement and rotation: geometric configurations, cracks pattern (interfaces labelled in bold black) and resultant forces for $\delta = 2$ cm (a), $\delta = 30$ cm (b) and for the maximum allowable displacement $\delta = 60$ cm (c). In (d), configuration and internal stress state obtained from 3DEC and corresponding to the maximum allowable displacement $\delta = 58$ cm. In (e), comparison among the PRD and 3DEC analyses: trend of the vertical (T_v) and horizontal (T_h) thrust (dimensionless with respect to the total weight of the structure) exerted by the third pillar.

below anymore (Fig. 17a) and the structure exhibits a zero-energy mode mechanism (Fig. 16b–c). It is worth to point out that the trend of the total potential energy provides a precise and accurate criterion to define the collapse state of the structure.

Furthermore, just after a small foundation settlement (δ = 1 cm), a mechanism involving a part of the structure forms, and it remains qualitative the same up to collapse takes place (Fig. 15). It is worth pointing out that the PRD method allows catching a typical behaviour of masonry structures [2]: the masonry structures are, in their initial and perfect (no cracks) configuration (e.g. Fig. 15a), statically indeterminate, but when they undergo a little foundation displacement (Fig. 15b), they accommodate this change with a

rigid macro-block partition of the structure and the moving part of the structure, defined by this partition, becomes statically determined. In our case, the moving part is the right side of the cathedral while its left side remains statically indeterminate (Fig. 21). This is also highlighted by the trend of the horizontal components of the thrust on the first and on the second pillar (Fig. 19b). For these pillars, the space of the dual problem is not a singleton, and for this reason, the curves representing the horizontal thrusts show many little jumps in each step. Instead, the horizontal thrusts exerted by the third and fourth pillars are smooth (except for some discrete jumps), showing that the solution space of admissible stress state (for the right part) is *very tight*. This suggests that the right part of the structure is statically determinate.

We show in Fig. 21 the six mechanisms used by the cathedral to accommodate the increasing foundation displacement until it collapses: the rigid macro-block partition (defined by a small number of rigid macro-blocks) can be easily recognised. This behaviour can also be seen from Fig. 22a, where the streamlines of the displacement field of the centroids of each block are plotted: most of the structure does not displace, whilst the part close to the third pillar is moving down accommodating the new boundary conditions with a quasi-smooth rigid displacement. This quasi-smooth rigid displacement can be recognisable from Fig. 22b where the vertical and horizontal displacements of the CPs defined in Fig. 17b are reported. Moreover, when the displacement reached the critical value of 181 cm, the horizontal displacement of CP2 moves up suddenly denoting that the central nave arch starts collapsing before the other elements.

In Fig. 23 the vertical and horizontal components of thrusts exerted by the structural elements identified in Fig. 17b are plotted: as expected the left and right horizontal components are the same.

Globally, the curves represented in Fig. 19 (the ones related to the PRD results) and in Fig. 23 show six jumps. Without considering the initial jump, occurring when the structure starts moving down ($\delta = 1$ cm) and the thrusts of the whole structure and of some elements drop down or increase suddenly, there are other five jumps. These jumps occur whether the mechanism switches from one configuration to another or if the internal stress state changes suddenly. In Fig. 24 the four changes are highlighted. The first jump, corresponding to a displacement δ in between 4 cm and 5 cm, occurs when the thrust line in the aisle arch switch suddenly from the configuration depicted in Fig. 24a to the one depicted in Fig. 24b. The second jump ($19\text{cm} \leq \delta \leq 20\text{cm}$) occurs when the thrust line in the central nave arch switch suddenly from the configuration depicted in Fig. 24c to the one in Fig. 24d. After some steps ($\delta = 49$ cm) a hinge compatible with the new location of the thrust line opens up on the left side of the central nave arch (Fig. 21b). This represents one of the peculiarities of the PRD approach: the forces can touch the boundary but a hinge forms if and only if the boundary conditions allow for a new configuration. Only if the structure (locally or globally) is collapsing (e.g. under

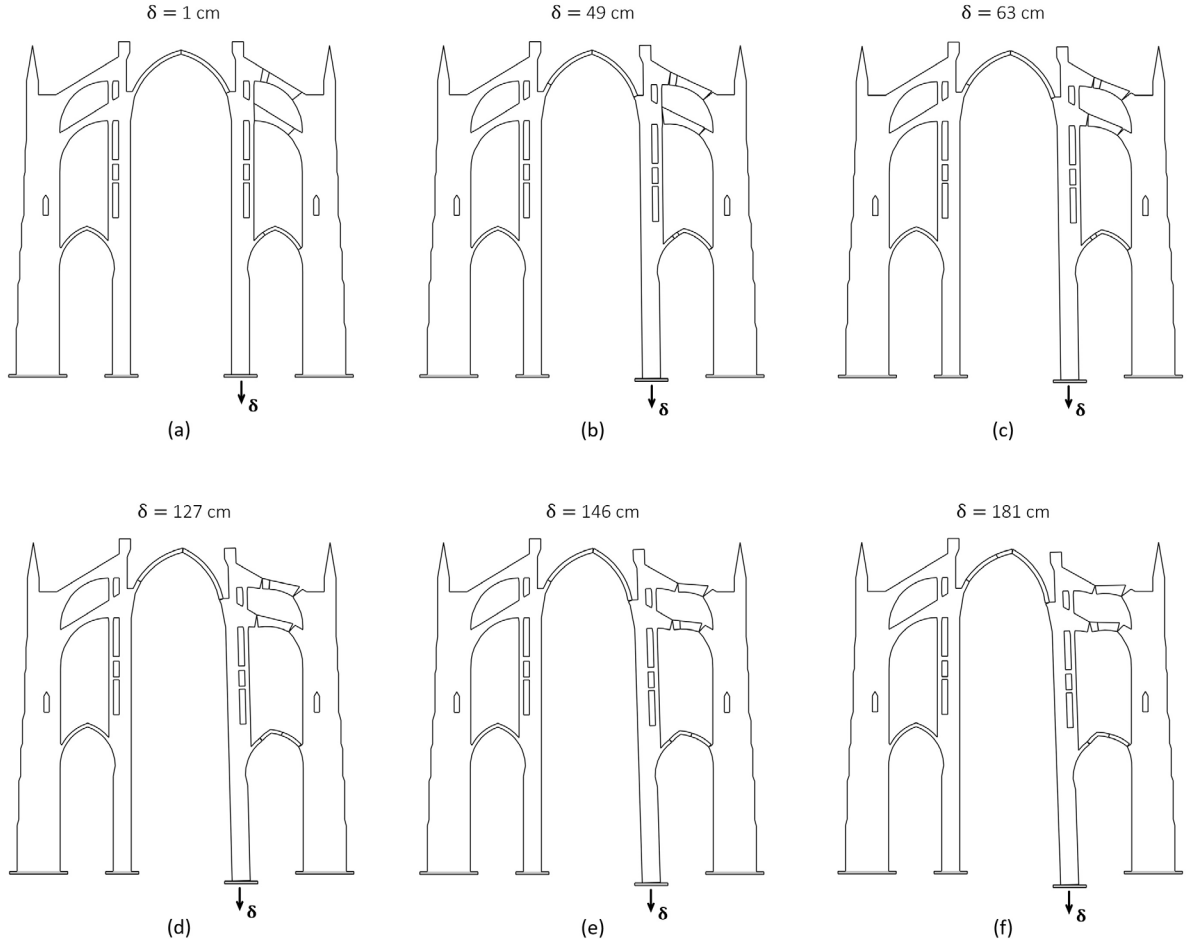

Fig. 21. The six different configurations defining the evolution of the mechanism until the structure collapses. Stable mechanism: (a–e), collapse mechanism: (f). The internal interfaces labelled in black are the ones affected by cracks. The crack pattern changes when the foundation displacement increases: new hinges open up while others close.

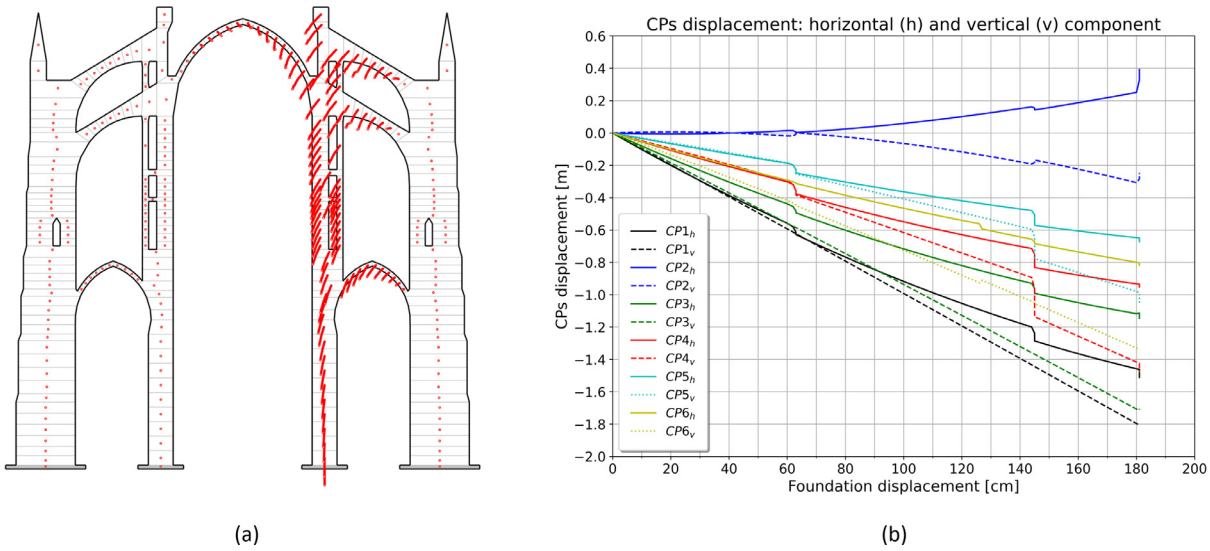

Fig. 22. Streamlines of the displacement field of the centroids of the blocks: red circles are used to denote the position of the centroids. Most of the structure is not moving, and the mechanism affects just the part close to the third pillar (a). Displacements of the control points (CPs) defined in Fig. 17**b** (b). (For interpretation of the references to colour in this figure legend, the reader is referred to the web version of this article.)

increasing loads) hinges can form without changes in the boundary conditions. It is worth to point out that there are no jumps connected to $\delta = 49$ cm because the change in the arch thrust has already occurred. The remaining three jumps are strictly connected not just to a change of the internal stress state but to a change of the stress state determined by the formation of a new mechanism, that is: the third jump (49 cm $\leq \delta \leq$ 53 cm) and the fifth jump (143 cm $\leq \delta \leq$ 145 cm) occur when the location of the hinges on the flying buttresses moves down as depicted in Fig. 24e–f and i–l respectively, while the fourth jump (125 cm $\leq \delta \leq$ 127 cm) occurs when the crack pattern of the aisle arch changes (Fig. 24g–h). The changes in the mechanisms can also be recognised in the displacement of the CPs from Fig. 22: particularly, the ones regarding the flying buttresses affect only the displace-

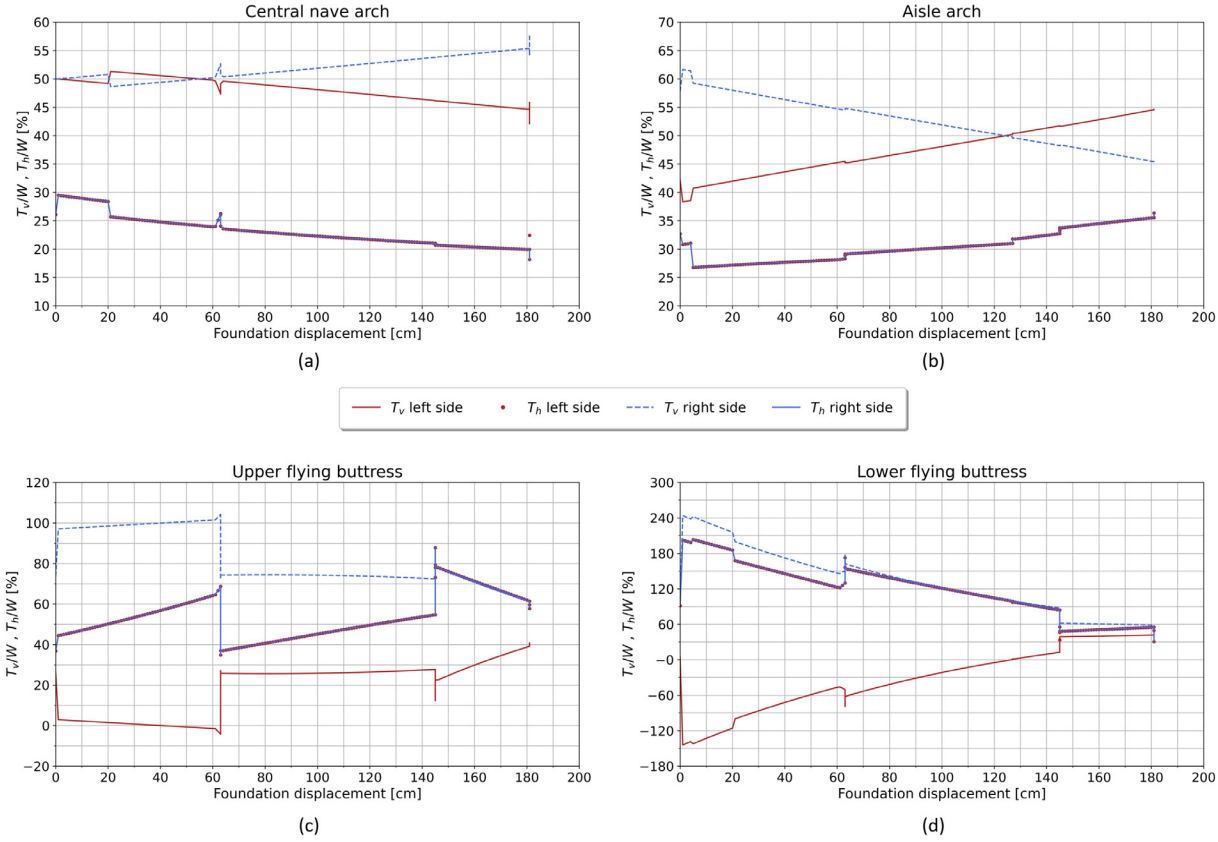

Fig. 23. Thrusts (dimensionless with respect to the element weight) exerted by the four structural elements depicted in Fig. 17b: central nave arch (a), aisle arch (b), upper (c) and lower (d) flying buttresses.

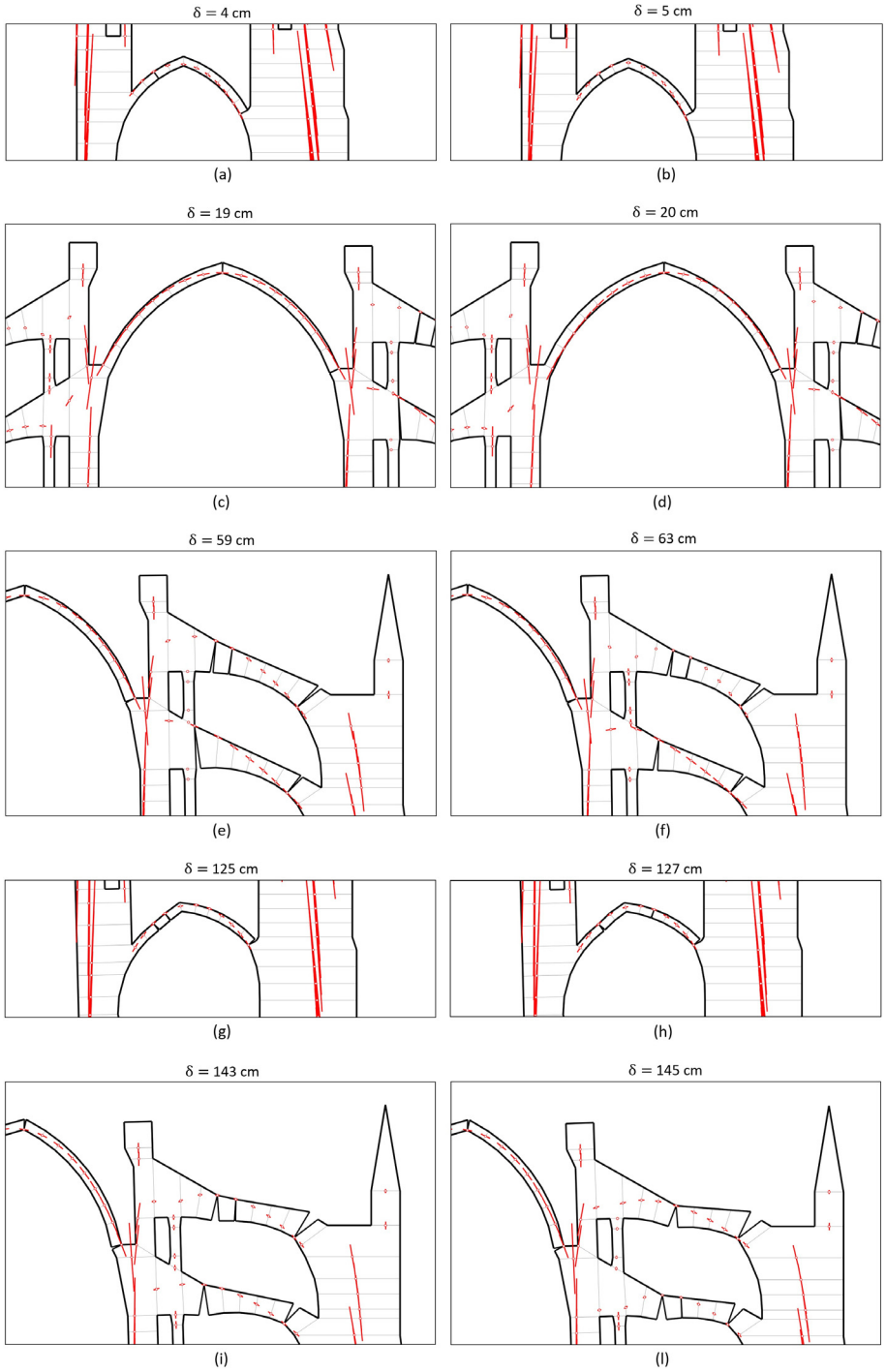

Fig. 24. Change of the internal stress state in the central nave arch: (a–b). Changes of the location of the hinges in the flying buttresses (c–d, g–h) and in the aisle arch (e–f). The resultant forces with their application points as well as the hinges (labelled in bold black) are depicted to visualise these changes more clearly.

ment of the CPs of the upper part of the structure (i.e. from CP1 to CP5) while the one regarding the change in the mechanism of the aisle arch can be seen only on the CP6 curve.

6. Conclusion

An extension of the PRD method to take into account the effects of large foundation displacements on the stability of masonry structures has been proposed. This extension allows coupling in a step-by-step procedure the original primal problem, proposed by the first author in [39] and with other co-authors in [40], with a new dual problem proposed for a continuum in [3] and formulated as an LP problem in [49]. The primal problem concerns the minimisation of the total potential energy, and its solution is represented by cracks (or mechanisms). In contrast, the dual problem regards the minimum of the complementary energy, and its solution allows finding internal and external forces in equilibrium with the external loads and compatible with the crack pattern. The proposed numerical approach allows to preserve the NRNT material restrictions on the deformed configuration and to frame the displacement capacity analysis as a sequence of LP problems written on the updated configuration in such a way that new hinges can form while old cracks can close: in the first case, the force goes

through the relative centre of rotation while in the second it is back to lie within the interface.

First, the simple case of a pointed arch has been proposed to compare the PRD displacement capacity analysis with the results obtained from physical tests and a DEM analysis done with *compas_dem* using 3DEC in the background as solver: a very good agreement in terms of cracks evolution, mechanisms, forces and displacement capacity has been found (Section 3.4).

After benchmarking the PRD method, a complex numerical application based on the cross-section of a Gothic cathedral has been proposed for showing the main peculiarities of the PRD approach. Even in this case the PRD analysis has been benchmarked with 3DEC, showing a good agreement in terms of displacement capacity, stress states and evolution of mechanisms (Section 4.4). The first outcome of the proposed approach is that the PRD method catches the typical behaviour of masonry structures: they are resilient to (even non-small) changes in the boundary conditions showing a considerable ductility (or flexibility) in terms of displacement capacity (i.e. 180 cm for the cathedral). Since hinges can open up or close, they accommodate large foundation displacements with an evolution of the crack pattern defining different mechanisms. Moreover, as shown, the PRD approach provides not merely the evolution of the mechanism, but it couples the mechanism with the internal stress state until the structure collapses. Moreover, we show how an energy criterion regarding the total potential energy can be adopted to define the collapse state of a structure accurately. Even though the PRD method provides a clear visualisation of the mechanism and of the location of the hinges, we showed how the analysis of the thrust exerted by some structural elements or the displacement of some control points provide a criterion for understanding the changes in the mechanism and in the internal stress state. Some further theoretical features caught out by the PRD method and perfectly fitting the spirit of Limit Analysis, should be highlighted:

- the PRD method allows assessing if the initial configuration is stable or not and the dual formulation can be still applied (the complementary energy is zero) providing one of the infinite internal stress states [49], so without having to apply a displacement;
- starting from the initial (perfect) configuration, when a small settlement occurs, a mechanism forms and the internal stress state change suddenly getting compatible with the location of the hinges;
- the relation between forces and fractures is reversed, and it is framed more naturally: a hinge opens up if and only if the force is touching the corner, and the displacement (caused by that opening) is compatible with the boundary condition (this does not regard the cases when the structure is not stable under given loads);
- since the problem is framed as a sequence of LP problems, the solution can be evaluated in a few seconds: the entire displacement capacity analysis performed on the approximate cross-section of Amiens cathedral takes less than 20 s; and,
- looking at Table 1, the fast computational solving provided by the PRD approach opens up the possibility of performing not just small-displacement inverse analyses [40] but also to consider large-displacement, inverse analyses, particularly when the foundation displacements or the size of the cracks cannot be considered *small* when compared to the overall size of the structure (the reader is referred to [40]).

In this sense, by adopting a displacement approach, the PRD method constitutes a fast computational application of Limit Analysis to masonry structures. An issue of the PRD approach is that it cannot take into account sliding directly; this feature (or "limitation") comes from one of the Heyman's assumption. However, we showed how, with an appropriate discretisation of the geometry (following the concept of stereotomy and of "*regola dell'arte*") the solutions are in perfect concordance with the ones obtained through DEM analyses, at least for friction angles greater than 35°, so for a reasonable value for the representative volume of masonry material.

Funding

This work was supported by the SNSF – Swiss National Science Foundation. Project grant n° 178953: "Practical Stability Assessment Strategies for Vaulted Unreinforced Masonry Structures".

Declaration of Competing Interest

The authors declare that they have no known competing financial interests or personal relationships that could have appeared to influence the work reported in this paper.

References

[1] Como M. Statics of historic masonry constructions. Berlin: Springer; 2013.
[2] Heyman J. The stone skeleton. Int J Solids Struct 1966;2(2):249–79.
[3] Angelillo M, Fortunato A, Gesualdo A, Iannuzzo A, Zuccaro G. Rigid block models for masonry structures. Int J Masonry Res Innov 2018;3(4):349–68.
[4] Ochsendorf J. The masonry arch on spreading supports. Struct Eng 2006;84 (2):29–34.
[5] Zampieri P, Zanini MA, Faleschini F, Hofer L, Pellegrino C. Failure analysis of masonry arch bridges subject to local pier scour. Eng Fail Anal 2017;79:371–84.
[6] Reccia E, Milani G, Cecchi A, Tralli A. Full 3D homogenization approach to investigate the behavior of masonry arch bridges: the Venice trans-lagoon railway bridge. Constr Build Mater 2014;66:567–86.
[7] Spada A. The effect of vertical ground movement on masonry walls simulated through an elastic–plastic interphase meso-model: a case study. Arch Appl Mech 2019;89(8):1655–76.
[8] Barentin CC, Van Mele T, Block P. Robotically controlled scale-model testing of masonry vault collapse. Meccanica 2018;53(7):1917–29.
[9] Van Mele T, McInerney J, DeJong MJ, Block P. Physical and computational discrete modeling of masonry vault collapse. In: Proceedings of the 8th international conference on structural analysis of historical constructions, SAHC 2012, 15–17 October, Wroclaw, Poland. p. 2252–560.
[10] McInerney J, DeJong MJ. Discrete element modeling of groin vault displacement capacity. Int J Architect Heritage 2015;9(8):1037–49.
[11] Simon J, Bagi K. Discrete element analysis of the minimum thickness of oval masonry domes. Int J Architect Heritage 2016;10(4):457–75.
[12] De Felice G, Malena M. Failure pattern prediction in masonry. J Mech Mater Struct 2019;14(5):663–82.
[13] Dell'Endice A, Iannuzzo A, DeJong M, Van Mele T, Block P. Modelling imperfections in unreinforced masonry structures: Discrete Element simulations and scale model experiments of a pavilion vault. Engineering Structures; 2020. submitted for review.
[14] Galassi S, Paradiso M, Tempesta G. Non-linear analysis of masonry structures subjected to external settlements. Open J Civil Eng 2013;3(02):18.
[15] Galassi S, Misseri G, Rovero L, Tempesta G. Failure modes prediction of masonry voussoir arches on moving supports. Eng Struct 2018;173:706–17.
[16] Gilbert M, Melbourne C. Rigid-block analysis of masonry structures. Struct Eng 1994;72(21).
[17] Livesley RK. A computational model for the limit analysis of three-dimensional masonry structures. Meccanica 1992;27(3):161–72.
[18] Portioli F, Cascini L. Assessment of masonry structures subjected to foundation settlements using rigid block limit analysis. Eng Struct 2016;113:347–61.
[19] Portioli F, Cascini L. Large displacement analysis of dry-jointed masonry structures subjected to settlements using rigid block modelling. Eng Struct 2017;148:485–96.
[20] Danyzy AAH. Méthode générale pour déterminer la résistance qu'il faut opposer à la poussée des voûtes. Histoire de la Société Royale des Sciences établie à Montpellier. vols. 2(1718–1745). p. 40–56. Published: Lyon 1778; 1732.
[21] Poleni G. Memorie istoriche della gran cupola del tempio Vaticano e de'danni di essa e detristoramenti loro, divisi in libri cinque, Padova: Nella stamperia del seminario; 1748.
[22] Fitchen J. The construction of Gothic cathedrals: a study of medieval vault erection. University of Chicago Press; 1981.
[23] Huerta S. The analysis of masonry architecture: a historical approach: to the memory of professor Henry J. Cowan. Architect Sci Rev 2008;51(4):297–328.
[24] Giuffrè A. Letture sulla Meccanica delle Murature Storiche. Edizioni Kappa 1991.

[25] Heyman J. The safety of masonry arches. Int J Mech Sci 1969;11(4):363–85.
[26] Heyman J. The gothic structure. Interdisc Sci Rev 1977;2(2):151–64.
[27] Huerta S. Galileo was wrong: the geometrical design of masonry arches. Nexus Netw J 2006;8(2):25–52.
[28] Block P, Ochsendorf JA. Thrust network analysis: a new methodology for three-dimensional equilibrium. J Int Assoc Shell Spatial Struct 2007;48(3):167–73.
[29] Kurrer KE. The history of the theory of structures: from arch analysis to computational mechanics. Int J Space Struct 2008;23(3):193–7.
[30] Ochsendorf JA. Collapse of masonry structures Doctoral dissertation:. University of Cambridge; 2002.
[31] Shin HV, Porst CF, Vouga E, Ochsendorf JA, Durand F. Reconciling elastic and equilibrium methods for static analysis. ACM Trans Graphics (TOG) 2016;35(2):13.
[32] Block P, Ciblac T, Ochsendorf JA. Real-time limit analysis of vaulted masonry buildings. Comput Struct 2006;84(29–30):1841–52.
[33] Zampieri P, Faleschini F, Zanini MA, Simoncello N. Collapse mechanisms of masonry arches with settled springing. Eng Struct 2018;156:363–74.
[34] Smars P. Etudes sur la stabilité des arcs et voûtes, KULeuven: PhD dissertation; 2000.
[35] Smars P. Kinematic stability of masonry arches. Adv Mater Res 2010;133:429–34.
[36] Block P, DeJong M, Ochsendorf JA. As hangs the flexible line: Equilibrium of masonry arches. Nexus Netw J 2006;8(2):13–24.
[37] Coccia S, Di Carlo F, Rinaldi Z. Collapse displacements for a mechanism of spreading-induced supports in a masonry arch. Int J Adv Struct Eng 2015;7(3):307–20.
[38] Hernando García J, Magdalena Layos F, Aznar López A. Cracking of masonry arches with great deformations: a new equilibrium approach. J Mech Mater Struct 2019;13(5):647–56.
[39] Iannuzzo A. A new rigid block model for masonry structures, Ph.D Dissertation, Università degli Studi di Napoli Federico II; 2017.
[40] Iannuzzo A, Angelillo M, De Chiara E, De Guglielmo F, De Serio F, Ribera F, et al. Modelling the cracks produced by settlements in masonry structures. Meccanica 2018;53(7):1857–73.
[41] Angelillo M. Constitutive relations for no-tension materials. Meccanica 1993;28:195–202.
[42] Angelillo M. Practical applications of unilateral models to Masonry Equilibrium. In: Angelillo M, editor. Mechanics of masonry structures. Vienna: Springer; 2014. p. 109–210.
[43] Angelillo M, Cardamone L, Fortunato A. A numerical model for masonry-like structures. J Mech Mater Struct 2010;5(4):583–615.
[44] Del Piero G. Limit analysis and no-tension materials. Int J Plast 1998;14(1–3):259–71.
[45] Tralli A, Chiozzi A, Grillanda N, Milani G. Masonry structures in the presence of foundation settlements and unilateral contact problems. Int J Solids Struct 2020;191:187–201.
[46] Iannuzzo A, De Luca A, Fortunato A, Gesualdo A, Angelillo M. Fractures detection in masonry constructions under horizontal seismic forces. Ingegneria Sismica 2018;35(3):87–103.
[47] Iannuzzo A, De Serio F, Gesualdo A, Zuccaro G, Fortunato A, Angelillo M. Crack patterns identification in masonry structures with a C° displacement energy method. Int J Masonry Res Innov 2018;3(3):295–323.
[48] Iannuzzo A. Energy based fracture identification in masonry structures: the case study of the church of "Pietà dei Turchini". J Mech Mater Struct 2019;14(5):683–702.
[49] Iannuzzo A, Van Mele T, Block P. Piecewise Rigid Displacement (PRD) method: a limit analysis-based approach to detect mechanisms and internal forces through two dual energy criteria. Mech Res Commun 2020;107:. https://doi.org/10.1016/j.mechrescom.2020.103557103557.
[50] De Serio F, Angelillo M, De Chiara E, Gesualdo A, Iannuzzo A, Pasquino M. Masonry structures made of monolithic blocks with an application to spiral stairs. Meccanica 2018;53(8):2171–91.
[51] Iannuzzo A, Olivieri C, Fortunato A. Displacement capacity of masonry structures under horizontal actions via PRD method. J Mech Mater Struct 2019;14(5):703–18.
[52] Van Mele T, et al. COMPAS: A framework for computational research in architecture and structures. https://doi.org/10.5281/zenodo.2594510, http://compas-dev.github.io/; 2017–2019.
[53] Iannuzzo A, Dell'Endice A, Maia Avelino R, Kao GTC, Van Mele T, Block P. COMPAS masonry: a computational framework for practical assessment of unreinforced masonry structures. In: Proceedings of the SAHC symposium: Barcelona; 2020.
[54] Iannuzzo A, Van Mele T, Block P. Assessment of unreinforced masonry structures through the PRD method. Int J Masonry Res Innov. IJMRI; 2020. Submitted for publication.
[55] Dell'Endice A, Iannuzzo A, Van Mele T, Block P. Influence of settlements and geometrical imperfections on the internal stress state of masonry structures. Proceedings of the SAHC symposium, 2020.
[56] Ambrosio L, Miranda Jr M, Pallara D. "Special functions of bounded variation in doubling metric measure spaces. Calculus Variations: Top Math Heritage E. De Giorgi 2004;1(45):14.
[57] Angelillo M, Babilio E, Fortunato A. Singular stress fields for masonry-like vaults. Continuum Mech Thermodyn 2013;25(2–4):423–41.
[58] Šilhavý M. Mathematics of the masonry–like model and limit analysis. In: Angelillo M, editor. Mechanics of masonry structures. Vienna: Springer; 2014. p. 29–69.
[59] Angelillo M, Babilio E, Fortunato A, Lippiello M, Montanino A. Analytic solutions for the stress field in static sandpiles. Mech Mater 2016;95:192–203.
[60] Lucchesi M, Šilhavý M, Zani N. A new class of equilibrated stress fields for no-tension bodies. J Mech Mater Struct 2006;1(3):503–39.
[61] Cundall PA. A computer model for simulating progressive large scale movements in blocky rock systems. In: Proceedings of the symposium of the international society of rock mechanics, Nancy, France; 1971.
[62] Forgács T, Sarhosis V, Bagi K. Minimum thickness of semi-circular skewed masonry arches. Eng Struct 2017;140:317–36.
[63] Lemos JV. Discrete element modeling of masonry structures. Int J Architect Heritage 2007;1(2):190–213.
[64] Forgács T, Sarhosis V, Bagi K. Influence of construction method on the load bearing capacity of skew masonry arches. Eng Struct 2018;168:612–27.
[65] Itasca Consulting Group, Inc. 3DEC, Three-Dimensional Distinct Element Code —, Ver. 5.2. Minneapolis: Itasca; 2016.
[66] Romano A. Modelling, analysis and testing of masonry structures, PhD dissertation: Università degli Studi di Napoli Federico II; 2005.
[67] Romano A, Ochsendorf JA. The mechanics of gothic masonry arches. Int J Architect Heritage 2010;4(1):59–82.
[68] Agrawal A, Verschueren R, Diamond S, Boyd S. A rewriting system for convex optimization problems. J Control Decis 2018;5(1):42–60.
[69] Mosek APS. The MOSEK optimization software. Online at http://www.mosek.com 2010; 54(2–1): 5.
[70] Mark R, Jonash RS. Wind loading on Gothic structure. J Soc Architect Historians 1970;29:222–30.
[71] Mark R. The structural analysis of Gothic cathedrals. Sci Am 1972;227(5):90–101.
[72] Croci G, Viskovic A, Sabbadini F. Some aspects of the structural behaviour of gothic cathedrals. In: Proc. IASS conf. spatial structures: past, present and future; 1995. p. 1207–14.
[73] Roca P, Cervera M, Pelà L, Clemente R, Chiumenti M. Continuum FE models for the analysis of Mallorca Cathedral. Eng Struct 2013;46:653–70.
[74] Heyman J. The structural engineer's view of ancient buildings. J Mech Mater Struct 2019;13(5):609–15.
[75] Huerta Fernández S. Geometry and equilibrium: the gothic theory of structural design. Struct Eng 2006;84(2):23–8.
[76] Fuentes P. Mechanics of flying buttresses: the case of the cathedral of Mallorca. J Mech Mater Struct 2019;13(5):617–30.
[77] Cennamo C, Cusano C. The gothic arcade of Santa Maria Incoronata in Naples: equilibrium of gothic arches. Int J Masonry Res Innov 2018;3(2):92–107.
[78] Coccia S, Como M, Di Carlo F. Wind strength of gothic cathedrals. Eng Fail Anal 2015;55:1–25.
[79] Kavanaugh C, Morris IM, Napolitano R, Jorquera-Lucerga JJ. Validating the use of graphical thrust line analysis for pier buttresses: The case study of Amiens cathedral. Int J Architect Heritage 2017;11(6):859–70.
[80] Viollet-le-Duc EE. Dictionnaire raisonné de l'architecture française du XIe au XVIe siècle. Paris: Morel; 1854–1866.
[81] Sarhosis V, De Santis S, de Felice G. A review of experimental investigations and assessment methods for masonry arch bridges. Struct Infrastruct Eng 2016;12(11):1439–64.